HHS Public Access

Author manuscript

Nat Metab. Author manuscript; available in PMC 2024 February 13.

Published in final edited form as:

Nat Metab. 2020 August ; 2(8): 703–716. doi:10.1038/s42255-020-0256-z.

Metabolic conditioning of CD8+ effector T cells for adoptive cell therapy

Ramon I. Klein Geltink[1,#,§], **Joy Edwards-Hicks**[1,#], **Petya Apostolova**[1], **David O'Sullivan**[1], **David E. Sanin**[1], **Annette E. Patterson**[1], **Daniel J. Puleston**[1], **Nina A.M. Ligthart**[1], **Joerg M. Buescher**[1], **Katarzyna M. Grzes**[1], **Agnieszka M. Kabat**[1], **Michal Stanczak**[1], **Jonathan D. Curtis**[1], **Fabian Hässler**[1], **Franziska M. Uhl**[2,3], **Mario Fabri**[1], **Robert Zeiser**[2], **Edward J. Pearce**[1,3], **Erika L. Pearce**[1,*]

[1]Max Planck Institute for Immunobiology and Epigenetics, 79108 Freiburg, Germany

[2]Department of Medicine I, Medical Center - University of Freiburg, Faculty of Medicine, University of Freiburg, Freiburg, Germany

[3]Faculty of Biology, University of Freiburg, 79104 Freiburg, Germany

Abstract

Effector $CD8^+$ T cell (T_E) proliferation and cytokine production depends on enhanced glucose metabolism. However, circulating T cells continuously adapt to glucose fluctuations caused by diet and inter-organ metabolite exchange. Here we show that transient glucose restriction (TGR) in activated $CD8^+$ T_E metabolically primes effector functions and enhances tumor clearance in mice. Tumor-specific TGR $CD8^+$ T_E co-cultured with tumor spheroids in replete conditions display enhanced effector molecule expression, and adoptive transfer of these cells in a murine lymphoma model leads to greater numbers of immunologically functional circulating donor cells and complete tumor clearance. Mechanistically, TGR T_E undergo metabolic remodelling that upon glucose re-exposure supports enhanced glucose uptake, increased carbon allocation to the pentose phosphate pathway (PPP), and a cellular redox shift toward a more reduced state, all indicators of a more anabolic program to support their enhanced functionality. Thus, metabolic conditioning could be utilized to promote efficiency of T cell products for adoptive cellular therapy.

Introduction

During T cell activation, metabolism is altered to increase glycolytic flux crucial to support T_E function [1–4]. When glucose is limiting, T_E rewire central carbon metabolism to sustain

*Correspondence should be addressed to: pearce@ie-freiburg.mpg.de.

§Present address: Department of Pathology and Laboratory Medicine, University of British Columbia/BC Children's Hospital Research Hospital, Vancouver, BC, V5Z 4H4, Canada

#Denotes equal contribution

Author Contributions

R.I.K.G, J.E.H., P.A., D.O.S., D.E.S, D.J.P., J.M.B., K.M.G, A.M.K., M.S., F.M.U., M.F., R.Z., E.J.P, and E.L.P designed research, analyzed data, and provided conceptual input. A.E.P., N.A.M.L., J.D.C, and F.H analyzed data and performed experiments. R.I.K.G, J.E.H. and E.L.P wrote the manuscript.

Competing Interests Statement

E.L.P. is an SAB member of ImmunoMet Therapeutics, and E.L.P and E.J.P. are Founders of Rheos Medicines. The other authors declare no competing interests.

survival, which is accompanied by reduced mTOR signaling [5], engagement of the cellular energy sensor AMPK [6], reduced proliferation, and elongation of mitochondria associated with higher mitochondrial spare respiratory capacity (SRC) in a CD28-dependent manner [7]. These mitochondrial changes in T cells are crucial for long-term protection against tumor recurrence [7–12], and augmented mitochondrial fitness can contribute to enhanced capacity to clear tumors [8,12]. In addition, glucose is crucial for optimal effector function *in vivo* and *in vitro*, and metabolic limitations contribute to dysfunction of T cells in the tumor microenvironment (TME) [13]. Short-term glucose depletion reversibly limits IFN-γ production in T cells [4], while, long-term glucose depletion is detrimental to T cell function and can lead to epigenetic modifications that cannot be reversed by glucose re-exposure [14]. Also, transient dampening of glycolysis during T cell activation is beneficial for the generation of long-lived memory T (T_M) cells, which leads to greater immune protection *in vivo* [9,10,15]. Like the effects of dampening glycolysis during activation, selecting cells with reduced mitochondrial membrane potential [10], or transient interference with glutamine metabolism during activation, benefits anti-tumor $CD8^+$ T cell responses [16].

Despite these observations, how T cells adapt to nutrients as they encounter substrate fluctuations remains unclear. To address the changes T_E undergo during temporary substrate limitation, we utilized transient glucose restriction (TGR) during which we monitored metabolic and functional changes. By re-exposing substrate-depleted T cells to glucose, we found that glucose carbon allocation was altered in cells after TGR. TGR led to greater anabolic engagement after glucose re-exposure, and was associated with better anti-tumor function *in vitro* and *in vivo*. Our results suggest that TGR treatment of fully activated $CD8^+$ T_E could benefit the *in vivo* functional capacity of T cells for adoptive cellular therapy in cancer.

Results

TGR enhances $CD8^+$ T_E cytokine production upon glucose re-exposure

To model the ability of TGR T_E to mount anti-tumor responses in the TME we generated spheroids of the murine melanoma cell line B16 expressing ovalbumin (B16-F10–0VA). Spheroids were established in T cell culture media for 7 days. OT-I splenocytes were activated with OVA-derived SIINFEKL peptide for 2 days followed by 24h expansion in IL-2. Cultures were then split into media containing either 10mM (control, black) or 1mM glucose (TGR, orange) for 20h (Fig. 1a). The control or TGR T_E were added to B16-F10-OVA spheroids in fresh media containing 10mM glucose and IL-2. 24h after co-culture the TGR T_E cells produced significantly more IFN-γ (Fig. 1b,c) both by level of IFN-γ production per cell (MFI, Fig. 1c left panel) and by percentage of IFN-γ positive cells (Fig. 1c right panel). In addition, the TGR T_E produced more granzyme B (GZMB) upon encountering OVA-positive tumor spheroids by MFI and percentage of $GZMB^{hi}$ expressing cells (Fig. 1b,d). Further addition of glucose did not increase effector molecule expression in either of the cell populations.

In the spheroid co-cultures, both control and TGR T_E experienced a comparable nutrient microenvironment with similar antigen exposure, suggesting that pre-treatment with TGR allows $CD8^+$ T_E to produce more effector molecules. To assess whether the enhanced

effects were cell-intrinsic, or caused by altered resistance to immunomodulatory signals from the tumor spheroids, we activated WT CD8$^+$ T cells with anti-CD3/28 in IL-2 for 48h, followed by expansion for 24h in IL-2. Like in Fig. 1a, the cultures were then exposed to either 10mM glucose (black) or TGR (orange) for 20h. Control or TGR T_E were re-stimulated with PMA-ionomycin in fresh media containing 10mM glucose and IL-2. TGR-T_E increased expression of granzyme B (Fig. 1e) and augmented IFN-γ production (Fig. 1f). Similarly, 2-deoxyglucose (2-DG)-mediated inhibition of glucose metabolism followed by 2-DG washout and re-stimulation with PMA-ionomycin in the presence of glucose augmented IFN-γ production (Fig. 1g, h). Thus, T cells transiently exposed to limiting glucose responded more vigorously to antigen re-stimulation, both in the context of tumor spheroids, or non-TCR-dependent stimulation by PMA/ionomycin, when exogenous glucose was replenished.

Given that T_M cells, including T_M-like cells generated with IL-15 in vitro, respond more vigorously to antigen [13] we assessed whether TGR induced a T_M-like phenotype in T_E during the 20h culture period. TRG T_E do not resemble memory-like T cells, suggested by their comparatively higher expression of the effector cell-surface markers CD25 (Fig. 1i) and CD98 (Fig. 1j), as well as the mTORC1 target p-4E-BP1 (Fig. 1k), when compared to T_E cells exposed to IL-15 for 20h.

TGR CD8$^+$ T_E have depleted sugar metabolism, but sustain mitochondrial activity

To assess metabolic changes, WT CD8$^+$ T cells were activated with anti-CD3/28 for 48h, expanded for 24h in IL-2, then exposed to 20h of 10mM glucose or TGR as before. Polar metabolites were extracted, followed by untargeted metabolomic analysis, which identified glucose and the aerobic glycolysis product lactate to be significantly lower in the TGR T_E (Fig. 2a). Kegg analysis showed that the significantly deceased metabolites in the TGR T_E were restricted to sugar metabolism intermediates and intermediates of the PPP (Fig. 2b). These observations suggested that the cells adapted to reduced glucose by limiting glucose-dependent anabolic processes, while maintaining allocation to metabolic pathways needed for survival. To assess whether the reduction in metabolite pool sizes was associated with differential glucose carbon allocation during TGR we incubated cells for 20h with uniformly-labeled (U^{13}C) glucose. Extracellular glucose was incorporated in a glucose concentration-dependent manner, confirming the reduction in pool sizes of central glycolytic intermediates as presented in Fig. 2a, b. We measured reduced glucose carbon allocation to glycolytic intermediates over the 20h of TGR (Fig. 2c, open bars), however, neither TCA intermediate pool sizes (Fig. 2d, open and closed bars), nor the percent allocation of ^{13}C label for 2 out of 3 TCA intermediates (Fig. 2e) were affected. Thus, glucose carbon allocation to the TCA cycle was maintained, even with limiting extracellular glucose and depletion of glycolytic intermediates. The preferential maintenance of glucose-derived TCA intermediates during TGR appeared sufficient as no compensatory increase in glutamine uptake from the media (Extended Data Fig. 1a) or glutamine carbon allocation to TCA intermediates (Extended Data Fig. 1b, open bars) were observed. Given the increased functional ability of TGR T_E in spheroid co-cultures, we also tested whether lactate, a metabolite present at high concentrations in the TME could be used as an alternative carbon source during TGR. Both control and TGR T_E incorporated lactate-derived carbons in the

TCA intermediate citrate to a similar degree, indicating that TGR T_E do not switch to lactate as an alternative substrate (Extended Data Fig. 1c).

To further assess global metabolic activity of T_E during TGR, we measured the effects of glucose starvation using extracellular flux analysis. We activated $CD8^+$ T cells in IL-2 followed by a 20h exposure to a glucose titration (Fig. 2f). We measured basal metabolism in unbuffered XF media with a titration of glucose matching the overnight cultures. Upon lowering glucose concentrations, we observed a shift in the relative metabolic state of the TGR cells, as assessed by the oxygen consumption rate (OCR) and extracellular acidification rate (ECAR) as a proxy for oxidative phosphorylation and lactate secretion from the cells, respectively. Basal OCR levels in TGR T_E were increased when glucose was limiting (Fig. 2g), whereas ECAR levels were reduced (Fig. 2h), as predicted by the reduced lactate pool (Fig. 2a) and glucose allocation to lactate (Fig. 2c). The relative shift to more mitochondrial activity (increased OCR, decreased ECAR) was consistent with the sustained allocation of glucose carbon to the TCA cycle (Fig. 2d, e). Taken together these data suggest that during TGR, $CD8^+$ T_E alter the allocation of acquired glucose carbons, dialing down the loss of carbons through the generation of the metabolic waste product lactate, and maintaining allocation to the TCA cycle, likely to increase energy efficiency and remain energetically viable.

To assess whether these metabolic alterations were mediated by global transcriptional changes we compared the single cell transcriptomes from control or TGR T_E (generated as in Fig. 2f) and found limited differences (Extended Data Fig. 2a). While there were significant changes in individual gene expression patterns between clusters (Extended Data Fig. 2b), Kegg pathway analysis did not detect central carbon pathway alterations, but flagged OXPHOS related gene expression as significantly regulated between clusters 0 and 1 (Extended Data Fig. 2c). There was a slight shift in the proportion of TGR T_E toward cluster 1, in agreement with the enhanced OCR (Fig. 2h). Although OXPHOS genes were altered, they related to ETC complexes, and while the OXPHOS module score between clusters did vary, it was not significantly driven by the control or TGR condition (Extended Data Fig. 2d). Therefore, we postulated that the altered metabolic state and glucose carbon allocation was likely not mediated by global transcriptional remodeling of T_E in response to TGR. To further highlight this, we compared expression of key enzymes that are involved in OXPHOS, glycolysis, and the PPP generated from the single cell data, which showed no significant differential expression between the two T_E cultures (Extended Data Fig. 2e).

$CD8^+$ T_E restore energetic balance during TGR

Since glucose is an important carbon source to generate energy in activated T cells [17], we assessed the activation state of AMP-kinase, an indicator of energy stress [18]. TGR T_E did not show enhanced AMPK phosphorylation after 20h, but rather a reduction in phosphorylation after TGR (Fig. 3a), suggesting that cellular energy homeostasis was not negatively affected. Also, despite lower available carbon substrate, we did not detect significant differences in ATP/AMP ratios in TGR T_E (Fig. 3b), suggesting that the amount of energy in TGR T cells was not rate-limiting, which was also consistent with the lack of compensation by glutamine metabolism (Extended Data Fig. 1). Given that previous studies highlighted

increased AMPK activity in T cells upon glucose depletion [5,6], we assessed the extracellular metabolite concentrations in the media in 2h intervals over the 20h window. While the control T_E had half the original concentration of glucose in the media after 20h, the TGR cultures depleted extracellular glucose after 12h (Fig. 3c). The glutamine concentration in the media was comparable between the two cultures (Fig. 3d), agreeing with the stable glutamine allocation in both cell types (Extended Data Fig. 1). Glucose consumption was mirrored by lactate production, which increased between cell types over the first 8 hours, but as glucose was depleted in the TGR cultures, lactate production plateaued (Fig. 3e).

To visualize both the acute and long-term effects of glucose depletion, we measured AMPK and mTORCI signaling pathways by western blot over the 20h culture. In response to metabolic stress, activated AMPK phosphorylates acetyl-coA carboxylase 1 (ACC1) on serine 79 [6]. Neither p-ACC nor p-AMPK was increased at 20 hours after TGR when compared to their levels earlier in the timecourse (Fig. 3f, Extended Data Fig. 3). AMPK phosphorylation did not precede the p-ACC signal in this setting (Fig. 3f, Extended Data Fig. 3). mTORCI signaling, visible as S6 phosphorylation, decreased after glucose depletion in the cultures. Although S6 phosphorylation was decreased at 20h in TGR T_E, we observed no phosphorylation differences of the direct mTORCI target 4E-BP1, which regulates CAP-dependent translation [22]. Despite being depleted of glucose, the TGR T_E increased over time glucose transporter GLUT1, a transporter induced by TCR signals that is important for T cell activation [19,20]. Our scRNA sequencing data did not identify Glut1 transcripts as differentially regulated between control and TGR T_E cultures, suggesting that Glut1 expression was post-transcriptionally regulated by glucose depletion in TGR cultures, perhaps as a stress response to be able to better compete for substrate. Taken together these data suggest that glucose depletion during TGR induced transient AMPK signaling, which is resolved after 20h in culture. Our data showing reduced AMPK signaling, maintained ATP/AMP ratios, and upregulated Glut1, indicate that TGR T_E cells restore energetic balance after the 20h culture period.

TGR T_E have decreased reducing equivalents, but do not accumulate ROS

To further assess T_E health, we measured the relative subcellular redox state in TGR T_E compared to control cells by exogenous expression of a targeted redox sensitive green fluorescent protein mutant (roGFP^{cyto}, cytosolic roGFP; roGFP^{mito}, mitochondrial roGFP (Fig. 4a,b) [23]. TGR T_E shifted to a more oxidized state in the cytosolic and mitochondrial compartments (Fig. 4b), along with a decreased GSH/GSSG ratio (Fig. 4c), although the NADH/NAD^+ ratio was not significantly altered (Fig. 4d). Many factors can influence the redox state of a subcellular compartment including the availability of reducing equivalents (NAD(P)H) or reactive oxygen species (ROS) [24–26]. Although the TGR T_E showed a more oxidized state, and presented higher basal mitochondrial activity (Fig. 2h), we did not detect an increase in cellular or mitochondrial ROS (Fig. 4e,f). The altered redox state might be explained by the altered glucose carbon allocation (Fig. 2b), the utilization of reducing equivalents to sustain complex I of the ETC (Fig. 2h), or the activity of ROS scavengers such as glutathione (GSH), which was also more oxidized (GSSG) in the TGR T_E, preventing the accumulation of ROS (Fig. 4c). Given the important role of GSH in T cell function [27], we measured the *de novo* GSH synthesis from U-^{13}C-glutamine during the 20h

culture period using m+5 labeled GSH. There was no significant difference in *de novo* GSH synthesis from glutamine between cultures (Fig. 4g), although there was an accumulation of m+10 GSSG (Fig. 4h). This suggests that although GSH synthesis from glutamine is not perturbed by TGR, the recycling of GSSG to GSH might be the reason for the altered GSH/GSSG ratio (Fig. 4c).

TGR CD8$^+$ T_E have enhanced anabolic metabolism upon glucose re-exposure

We assessed the effects of TGR on glucose metabolism when T_E were re-exposed to glucose. It was evident that stimulated TGR T_E were better equipped to produce effector molecules in higher glucose concentrations (Fig. 1). We asked whether glucose metabolism after glucose re-exposure was altered after TGR, perhaps mediating the augmented function. We activated, expanded, and glucose-restricted WT CD8$^+$ T cells as in Fig. 3a, and then performed extracellular flux analysis as in Fig. 3b. After baseline measurements of both OCR and ECAR in the context of a glucose titration, we exposed cells to 10mM glucose. TGR T_E increased glycolytic reserve (ECAR after oligomycin injection) (Fig. 5a), and decreased OCR (Fig. 5b, orange lines). These data showed that glucose re-exposure rapidly reversed the higher mitochondrial activity of TGR T_E (Fig. 2h), with a slight increase in the generation of glucose-derived lactate (ECAR) over the 30-minute window after glucose addition. The slight increase in ECAR and decrease in OCR after glucose addition was not evident in T_E exposed to control glucose concentrations from the beginning of the assay (black lines).

Since we observed a reduction in reducing equivalents upon glucose depletion (Fig. 4c) and a shift to an oxidized redox state (Fig. 4a,b), we asked if glucose re-addition would impact cellular redox. We observed a rapid reversal toward a reduced redox state in TGR T_E following glucose re-exposure (Fig. 5c). This glucose-mediated induction of a reduced cytosolic redox state could be a result of altered glucose carbon allocation, leading to the regeneration of reducing equivalents [25]. To evaluate whether TGR T_E allocate glucose carbon differently upon glucose re-exposure, we pulsed control or TGR T_E with 10mM U-^{12}C-glucose or U-^{13}C-glucose for 5 minutes followed by an untargeted analysis of the polar metabolome using XCMS [28], or X13CMS [28,29] software, respectively. By overlaying Kegg pathway hits derived from data of significantly increased total metabolite pools (Extended Data Fig.4a) and ^{13}C-isotope incorporation (Extended Data Fig. 4b), we found anabolic pathways, including the PPP and pyrimidine metabolism, to be enriched in refed TGR T_E (Fig. 5d and Extended Data Fig. 4c). To test assimilation of glucose carbons into these anabolic intermediates, we pulsed control T_E and TGR T_E with 10mM U-^{13}C-glucose followed by isotope tracing into glycolytic and PPP intermediates. By extracting metabolites at 30, 60, and 300 seconds after U-^{13}C-glucose addition we could establish enhanced accumulation of glucose-derived carbons in TGR T_E in intracellular glucose, and assimilation into glycolytic intermediates glucose-6P, and triose-P, but not lactate, at these early timepoints (Fig. 5e, orange open bars). The TGR T_E shunted glucose carbons into the NAPDH-regenerating oxidative PPP as shown by labeled pentose-P, and the non-oxidative PPP, by labelled sedoheptulose-P and erythrose-P (Fig. 5e, open orange bars). The enhanced carbon allocation to the PPP in TGR T_E was also evident in the enhanced NADPH regeneration (Fig. 5f, left panel) and drop in NADP pools (Fig. 5f, right panel), which could

in part be responsible for, and in agreement with, the reversal of the cytosolic redox state (Fig. 5c). The observed redox state reversal was also evident in the increase of GSH/GSSG ratio (Fig. 5g), but not in the NADH/NAD^+ ratio which changed neither during TGR (Fig. 4d), nor after glucose re-exposure (Fig. 5h).

Given the allocation to the PPP shortly after glucose re-exposure (Fig. 5e, orange open bars), we measured glucose carbon allocation in PPP-generated nucleotides. 6h after glucose re-exposure, TGR cells synthesized significantly more AMP, and UMP (Extended Data Fig. 5a, orange open bars), and the TGR T_E also made more ATP with glucose-derived carbons (Fig. 5i, orange open bars). In agreement with enhanced glucose anabolism, 6h after refeeding we there was an increase in glucose allocation to the amino acid serine (Extended Data Fig. 5b), important for T cell proliferation [30]. Although glucose carbon allocation into the PPP could be driven by the altered redox state, the normalized redox balance in TGR T_E 5 minutes after glucose re-exposure (Fig. 5g) remained stable after 6h, as suggested by a comparable GSH/GSSG ratio at this time point (Extended Data Fig. 5c), suggesting that the anabolic regulation might be impacted by other factors than solely redox balance.

To assess the functional relevance of the PPP in the TGR-mediated enhanced effector function (Fig. 1), we treated control and TGR cultures with the PPP inhibitor 6-aminonicotinamide (6-AN), followed by PMA/ionomycin restimulation. 6-AN treatment significantly blocked GZMB expression (Fig. 5j) and blunted IFN-γ expression (Fig. 5k), highlighting an important functional role for the enhanced PPP allocation. To determine the role of AMPK signaling in glucose-carbon allocation to the PPP after TGR (Fig. 3a, f), we inhibited AMPK with Compound C during glucose re-exposure. Glucose-carbon allocation to the PPP was similar between TGR T_E and untreated controls (Fig. 5l). Taken together these data suggest that TGR induces metabolic reprogramming leading to sustained anabolic metabolism upon activation and glucose re-exposure, further underwritten by significantly reduced lactate pools even 6h after glucose re-exposure (Extended Data Fig. 5d).

TGR enhances tumor-specific $CD8^+$ T_E function *in vivo*

Previous studies have highlighted the importance of enhanced mitochondrial metabolism [7–12], SRC [7,8] and dampened glucose metabolism during activation for the prolonged *in vivo* function of anti-tumor $CD8^+$ T_E [9,10,31]. TGR T_E presented with sustained mitochondrial metabolism (Fig. 2), enhanced SRC [7], altered redox state without augmented ROS (Fig. 4), and enhanced capacity to engage anabolism upon glucose re-exposure (Fig. 5). To ask whether TGR could condition *ex-vivo* generated antigen-specific $CD8^+$ T_E cells for enhanced efficacy of adoptive cellular therapy, we performed adoptive T cell transfers of TGR and control T_E into mice bearing EL4-OVA lymphoma tumors on their flanks (Fig. 6a). By injecting suboptimal numbers of T cells (3×10^6 per mouse) after the tumors had already established (day 8 post-injection, 8mm diameter average, Fig. 6b) we achieved a model by which the control T_E were able to control ~50% of the tumors with responses ranging from tumor clearance (black lines reverting to non-measureable tumors), stable disease control (no further increase or reduction in tumor size), to 4/9 mice showing limited tumor control followed by progressive disease, ultimately leading to mice having to be sacrificed (Fig. 6b, black lines). Strikingly, injection of 3×10^6 TGR T_E per mouse cleared

tumors in 10/10 mice (Fig. 6b, orange lines). These data demonstrated that TGR treatment augmented *in vivo* protective immunity against tumors. We bled the tumor bearing mice 8 days after T cell transfer (16 days post-tumor inoculation) and observed significantly higher numbers of circulating donor $CD8^+$ T cells in all mice receiving TGR T_E (Fig. 6c), despite the loss of tumor mass in all of the TGR T_E recipient mice (Fig. 6b, orange lines). In addition, circulating TGR T_E donor cells showed higher percentages of IFN-γ producers when re-stimulated *ex vivo* 8 days post-transplantation (Fig. 6d flow panels, quantified in Fig. 6e left panel), although there was no significant difference between subgroups in MFI of the IFN-γ expression (Fig. 6e right panel). When mice were bled 20 days after T cell transfer (28 days post-tumor inoculation), the augmented numbers of TGR T_E donor cells were persistent (Fig. 6f). Together these data suggested the better persistence and enhanced function of anti-tumor TGR T_E provided greater protection against tumor recurrence.

To extend our findings we tested the added benefit of TGR T_E in a murine melanoma model, in which we administered anti-PD-L1 checkpoint-therapy to mice bearing B16-F10-OVA flank tumors. T cell infusions of TGR T_E or control T_E were combined with 3 intraperitoneal injections with anti-PD-L1 or isotype control antibodies (Fig. 6g). We observed increased circulating donor-derived T cells in the TGR conditions as compared to controls 16 days post T cell infusion (Extended Data Fig. 6a). While adoptive transfer of donor-derived control or TGR T_E led to better tumor control compared to isotype only treated mice, TGR T_E (Fig. 6h orange squares) significantly slowed tumor progression compared to the control T_E (Fig. 6h black squares). These findings agreed with our previous *in vivo* experiments using EL4-OVA tumors both in terms of increased circulating numbers (Fig. 6c,f) and increased tumor control (Fig. 6b) in the TGR T_E condition.

Anti-PD-L1 therapy significantly improved tumor control in the control T_E recipient mice (Fig. 6i, black squares), but anti-PD-L1 therapy did not further improve the enhanced tumor control mediated by TGR T_E (Fig. 6i, orange squares). The increase in numbers of donor-derived TGR T_E cells was not only evident in the circulation (Extended Data Fig. 6a), but also in the tumors 16 days after T cell infusion (Fig. 6j,k left groups). Although TGR enhanced donor-derived T cells in circulation, independent of PD-L1 treatment (Extended Data Fig. 6a), the TGR-mediated enhanced number of donor-derived T cells inside the tumors was no longer evident when combined with anti-PD-L1 treatment (Fig. 6j,k right groups). Note that the percentage of donor-derived $CD8^+$ T cells is lower in the case of anti-PD-L1 treatment (Fig. 6k), reflecting the enhanced tumor-infiltration of host $CD8^+$ T cells after anti-PD-L1 treatment (Extended Data Fig. 6b). Taken together, these data suggest that 1) TGR leads to an augmented number of circulating donor-derived T cells increasing the likelihood of anti-tumor immunity. 2) TGR leads to an enhanced ability to infiltrate or survive inside B16-F10-OVA tumors. 3) This TGR-mediated increased ability to infiltrate or survive in the tumor was not further enhanced by anti-PD-L1 treatment.

Discussion

Previous studies have highlighted the benefit of blunting glycolysis during T cell activation on the development of long-lived functional memory T cells [9,10,31]. Aerobic glycolysis is a hallmark of fast-dividing cells [32,33], and dampening this pathway can be associated with

slower proliferation [34]. Rather than limiting glucose during activation, we depleted glucose after the cells engaged multiple rounds of division and were fully activated. Although this was associated with reduced proliferation over 20h of glucose-restriction, expansion in glucose-replete media before TGR allowed us to generate large numbers of activated $CD8^+$ T_E. This approach might be valuable in the generation of T cell products for adoptive cellular therapy, especially given the large numbers of cells infused into patients [35].

After acute glucose starvation *in vitro*, $CD8^+$ T cells become energetically stressed, as shown by activation of the energy sensor AMPK [5,6], which is also associated with dampened S6 phosphorylation and Glut1 upregulation (Fig. 3f). However, after TGR $CD8^+$ T_E had lower p-AMPK compared to control cells, and a non-significant, but reproducible increase in the ATP/AMP ratio (Fig. 3e), suggesting that TGR T_E have an improved energetic balance, and increased Glut1 expression, which may underlie their ability to robustly respond to glucose re-exposure. Although AMPK inhibition did not alter glucose carbon allocation upon refeeding, how the transient induction of AMPK activity and gradual upregulation of GLUT1 contributes to this phenotype is to be determined. Decreased ACC1 phosphorylation and GLUT1 upregulation coincide with the time that extracellular glucose is depleted, and could indicate that this is the metabolic switch leading to the adaptation observed at the 20h time point.

The sustained energy homeostasis in TGR T_E could in part be explained by their enhanced mitochondrial metabolism. Although we observed decreased metabolite pools in pathways associated with sugar metabolism, including amino- and nucleotide-sugar metabolism, and glycolysis, TCA metabolites did not decrease to the same extent. As the relative incorporation of glucose and glutamine carbons remained stable, we inferred that the T cells specifically allocated remaining glucose carbons away from anabolic pathways to sustain mitochondrial ATP production. Preferential glucose carbon allocation into the TCA cycle allows the full oxidation and generation of up to 10-fold more ATP per glucose molecule when compared to aerobic glycolysis. Another explanation for the sustained ATP pools is that TGR T_E do not have sufficient substrate for proliferation and cytokine production and therefore have a reduced ATP demand to fuel T_E functions.

Along with sustained ATP pools, the ability to handle oxidative stress is important for cellular health. While mitochondrial ROS is crucial for T cell activation [27,36], ROS accumulation can cause damage, leading to functional perturbation or programmed cell death [37]. Although TGR led to the relative oxidation of both the cytosolic and mitochondrial compartments, TGR T_E did not deplete the ROS scavenging molecule glutathione, in part supported by sustained glutathione synthesis from glutamine (Fig. 4g, h). This in combination with sustained reducing equivalents could be the metabolic rewiring that TGR T_E utilize to maintain basal metabolic activity in the cell, and then benefit from when carbons become available upon glucose re-exposure. A previous study highlighted that the accumulation of the redox co-factor NAD^+ allowed increased anti-tumor function of pro-inflammatory $CD4^+$ T cells [38]. A longer window of TGR could lead to depletion of these factors and lead to dysfunction that is no longer responsive to glucose re-exposure [14].

The differences in glucose carbon allocation after TGR showed that depletion of a dominant biofuel alters allocation of the same biofuel when re-encountered (Fig. 5e). Whether altered carbon allocation is a mediator of increased anti-tumor functions after glutamine depletion has not yet been addressed [16,39]. Redox state changes, as measured by roGFP and ratios of redox pairs, could account for this altered carbon allocation, as there is a depletion of redox cofactors no longer allowing reducing reactions to take place. Whether this is the cause or effect of altered glucose metabolism induced by TGR remains undetermined. The enhanced glucose carbon allocation into the PPP upon glucose re-addition could be supported by the accumulated $NADP^+$ in the TGR T_E (Fig. 5f). The concomitant increase in NADPH and decrease in $NADP^+$ upon glucose re-exposure could result from the allocation of glucose carbons to the PPP, as measured by increased levels of pentose-P derived from newly added glucose (Fig. 5e, open bars). This is also corroborated by the observed normalization of the GSH/GSSG ratios after glucose re-exposure.

How the enhanced carbon allocation to the oxidative and non-oxidative PPP augments effector function remains unclear. While PPP inhibition with 6-AN dampened TGR T_E cytokine production, PPP engagement is unlikely the sole contributor to enhanced function in vivo. Glucose 6-phosphate dehydrogenase (G6PD) inhibition abrogates pro-inflammatory cytokine production in $CD8^+$ T cells, in part by reduced IFN-γ transcription [40]. While this study links the PPP to cytokine production upon activation, other studies have shown that the flux through glycolysis is important for cytokine production. The dampened ability of T_E cells to produce IFN-γ in the absence of glucose [14], or when exposed to galactose [4], which enhances PPP flux and mitochondrial metabolism, suggests that hyperactivation of the PPP alone cannot compensate for a lack of glycolytic flux. A lack of increased IFN-γ transcription suggests a role for either NADPH or the biosynthetic contribution of the PPP in the augmented function of the TGR cells, but will require further investigation.

OT-I transgenic TGR T_E co-cultured with OVA-expressing B16 spheroids displayed increased anti-tumor immune function, as measured by effector molecule expression. The T_E were added to complete media containing IL-2, so the extracellular environment was identical in the cocultures. By using transgenic OT-I $CD8^+$ T_E, we normalized the TCR signal the cells received from the tumor cells. Regardless, effector cytokine production was augmented in the T_E exposed to TGR for 20h preceding the coculture, suggesting differences in cell-intrinsic metabolic signals associated with enhanced anti-tumor function. A recent study demonstrated that $CD8^+$ T cells activated *in vivo* shed fewer carbons as lactate and had greater glucose carbon allocation to anabolic pathways and the TCA cycle compared to T cells activated in vitro [41], suggesting that our TGR protocol may prepare cells for a more '*in vivo*-like' environment. Results showing that glucose only accounts for 10% of the biomass in actively proliferating lymphocytes [17] could therefore suggest that *in vitro* conditions lead to T cells being wasteful, no longer optimally utilizing the substrates that are plentiful in media.

Our data suggest that human T cell expansion protocols, such as those used for tumor-infiltrating lymphocyte (TIL) or CAR T cell therapy [42], could be amended to include a transient glucose starvation before transplantation. We reproducibly observed significantly more circulating donor cells after 8- and 20-days post-transplantation in mice, suggesting

that TGR confers survival and/or proliferative advantages to the cells after infusion. In addition to the increase in circulating donor-derived tumor-specific T cells, we also detected higher percentages of IFN-γ expressing cells that produced more GZMB upon *ex vivo* re-stimulation. The enhanced tumor clearance reflected the observation that not only *ex vivo* reactivation, but also *in vivo* function of these cells was significantly enhanced, leading to 100% tumor clearance in the EL4-OVA bearing mice receiving TGR-treated cells. Data from the B16-F10-OVA melanoma model suggested that this difference in tumor control is perhaps not solely due to enhanced anti-tumor function and *in vivo* persistence, but also increased tumor infiltration. Although we did not observe further therapeutic benefit by combining anti-PD-L1 therapy with TGR T_E adoptive transfer, the TGR T_E showed enhanced persistence in these mice as well. Future studies could determine which parameter is the driving force behind the anti-tumor activity and *in vivo* persistence observed after treating T_E with 20h TGR before infusion, but it is likely to be a combination of factors. Previous studies in murine tumor models identified that anti-PD-L1 therapy-induced increased respiration, and SRC, supporting enhanced tumor infiltration and CD8-mediated tumor control [12,43,44]. Comparably, TGR increases respiration (Fig. 2h), SRC [7], and tumor infiltration (Fig. 6j,k) perhaps explaining the lack of further therapeutic benefit of the anti-PD-L1 therapy on TGR T_E-infused mice.

We suspect that there is a limited time during which T cells can respond vigorously to added glucose. In a recent study we showed that prolonged glucose-restriction leads to epigenetic remodeling through loss of acetyl-CoA pools [14]. Whereas the cells undergoing transient starvation reacted vigorously to newly added glucose, when the depletion of extracellular glucose was prolonged for days, cells failed to augment effector cytokine production upon re-addition of glucose. These data showed that there is a window of opportunity to reinvigorate $CD8^+$ T_E upon transient glucose deprivation. We found that transient glucose-depletion after activation leads to metabolic reprogramming of $CD8^+$ T_E, enhancing their longevity and functional capacity *in vivo*. Our study highlights that dynamic changes in nutrient allocation are associated with functional outcomes in primary cells.

Further information and requests for resources and reagents should be directed to and will be made available upon reasonable request by the corresponding author, Erika L. Pearce (pearce@ie-freiburg.mpg.de).

Methods

Mouse lines

C57BL/6J (RRID: IMSR_JAX:000664), major histocompatibility complex (MHC) class I-restricted OVA specific TCR OT-I transgenic mice (RRID: IMSR_JAX:003831), $CD45.1^+$ C57NL/6J (B6.SJL-*Ptprc*^{a} *Pepc*^{b}/BoyJ; Jax, 002014) and Thy1.1 congenic (Jax strain number 000406) mouse strains were purchased from The Jackson Laboratory and were maintained at the Max Planck institute for Immunobiology and cared for according to the Institutional Animal Use and Care Guidelines. Tumor studies were approved by the animal care committee of the Regierungspraesidium Freiburg. Mice were bred under specific pathogen free standards, and transferred to open top cages for experimental procedures. For tumor experiments 9-11-week-old female mice were randomized to match age across

experimental groups. Temperature and humidity of the holding rooms was monitored daily and Tumor bearing mice were weighed every 2 days. Mouse body condition score was monitored over the experimental period, assuring the mice maintained expected weight gain, did not show signs of distress, tumors did not ulcerate and tumor size did not interfere with feeding or drinking of the animals and did not exceed 20mm diameter. No association between age or weight with response was observed or expected.

Primary T cell cultures

$CD8^+$ T cells were obtained from spleens and lymph nodes isolated from 8-12-week-old C57Bl/6 mice using the EasySep CD8 T cell isolation kit (Stem Cell technologies catalogue # 19753) according to the manufacturers protocol. Within experiments mice were age and sex matched. Sample size is indicated in the figure legends. Isolated T cells were activated using plate bound anti-CD3 (5 μg/ml) (InVivoMab anti-mouse CD3, BioXCell catalogue #BE0002); and soluble anti-CD28 (0.5 μg/ml) (InVivoMab anti-mouse CD28, BioXcell catalogue # BE0015), in 1640 media (invitrogen) supplemented with 10% fetal calf serum (Gibco), 4mM L-glutamine, 1% penicillin/streptomycin, 100 U/ml hrIL-2 (Peprotech), 55 μM beta-mercaptoethanol, in a humidified incubator at 37°C, atmospheric oxygen supplemented with 5% CO_2. For OT-I cultures, single cell suspensions of splenocytes were incubated for 48 hr in IL-2 containing media as above in the presence of SIINFEKL peptide. 48 hours after activation, media was replaced with expansion media containing 11mM glucose and 100U/ml IL-2. After 24 hours of expansion, cells were exposed to experimental media for 20 hours, containing a dilution series of glucose as indicated in figure legends (control $U^{12}C$ or stable isotope $U^{13}C$ to assess carbon allocation). Cells exposed to limiting glucose allocation (1mM) were plated at 1.5×10^6/ml to achieve equal cell number / ml after 20 hours for analysis of acute carbon allocation over time. For acute carbon allocation, 5×10^6 T cells/mouse/glucose concentration/time point were added to 5ml Eppendorf Safe-Lock tubes, and incubated in a 37°C aluminum bead bath. 10mM glucose (control $U^{12}C$ for pool size measurements or stable isotope $U^{13}C$ to assess glucose carbon allocation) was added to the cells, mixed and incubated for 30, 60, or 300 seconds followed by transfer to a watery ice bath to instantly cool the cultures. For stable isotope tracing, cells were incubated in differential U-^{13}C-glucose, U-^{13}C-glutamine or U-^{13}C-lactate for 6 or 20 hours as indicated in the figure legends. Pharmacological inhibition of glycolysis in T_E cells was achieved by treatment with low dose 0.5mM 2-deoxy-glucose (Sigma, L07338.14) or solvent (media) control for 20h, followed by drug washout and restimulation with PMA/ionomycin, as indicated in the figure legend. To block the PPP during glucose reexposure, cells were pretreated with 250μM 6-aminonicotinamide (Sigma, A68203) or solvent (DMSO) control for 30 minutes, followed by PMA/ionomycin restimulation as indicated in the figure legends. For AMPK pathway assessment TGR T_E cells were pretreated with 10μM Compound C (Merck, 171260) or solvent (DMSO) control for 30 minutes, followed by a 5 minute pulse with $U^{13}C$ glucose as indicated in the figure legend.

Metabolite extraction

Cells were collected by centrifugation at 4°C, washed in ice cold PBS, and polar metabolites were extracted twice using 500μl ice cold extraction buffer (50:30:20,

methanol:acetonitrile:water) (extraction buffer was pre-cooled on dry ice for 30 mins before extraction). Samples were centrifuged at maximum speed for 10 minutes to remove protein debris, and extracts were dried using an EZ2-Elite evaporator (Genevac). Metabolites were resuspended in 50ul extraction buffer and and stored at −80°C until acquisition.

Metabolite measurement by LC-MS

LC-MS was carried out using an Agilent 1290 Infinity II UHPLC inline with a Bruker Impact II QTOF operating in negative ion mode. Scan range was from 20 to 1000 Da. Mass calibration was performed at the beginning of each run. LC separation was on a Phenomenex Luna propylamine column (50 × 2 mm, 3 um particles) using a solvent gradient of 100% buffer B (5 mM ammonium carbonate in 90% acetonitrile) to 90% buffer A (10 mM NH4 in water). Flow rate was from 1000 to 750 uL/min. Autosampler temperature was 5 degrees and injection volume was 2uL.

Data analysis of metabolite measurements

For targeted analysis, metabolites were quantified using AssayR [45], and identified by matching accurate mass and retention time to standards. For untargeted analysis, samples were compared using XCMS [28], or X13CMS [29] (isotope-labeled samples), and significantly different metabolite identities (p-value cutoff <0.05) were defined by accurate mass using the Human Metabolomics Database (HMDB). For pathway analysis, metabolites assigned a Kegg ID in the HMDB were searched using the Kegg Mapper-Search Pathway tool. Kegg Pathways were ranked according to the number of metabolite hits in that pathway (from highest to lowest). Metabolites in the highest ranked pathways were further validated by targeted analysis.

Extracellular flux analysis (Seahorse assays)

Extracellular acidification rate (ECAR) and oxygen consumption rate (OCR) were measured using a Seahorse XFe96 bioanalyzer (Agilent). 2×10^5 T cells per well (minimum 3 wells per sample) were spun into previously poly-D-lysine coated seahorse 96 well plates and preincubated CO_2-free 37°C incubator for a minimum of 45 min. Basal OCR and ECAR were measured in cells incubated in unbuffered 1640 media supplemented with 1 mM pyruvate and 4 mM L-glutamine adjusted to pH 7.4 (for detailed protocols see ref [46]) in the presence of differential glucose concentrations, followed by the addition of 10 mM glucose, 1 μM oligomycin, and 50 mM 2-deoxyglucose (2-DG) (all Sigma) as indicated.

Cell lines

The murine EG.7 lymphoblast cell line expressing OVA (EL4-OVA; E.G7-OVA), was purchased from ATCC (ATCC Cat# CRL-2113, RRID: CVCL_3505), cultured for three passages before being implanted in the flank of naive mice. The murine melanoma cell line B16-F10-OVA was a kind gift of Dr. Dietmar Zehn. Further authentication of the cell lines was not performed. Cells were maintained in 1640 media (E.G7-OVA) or DMEM media (B16-F10-OVA) supplemented with 10% fetal calf serum, 4 mM L-glutamine, 1% penicillin/streptomycin, 55 μM beta-mercaptoethanol, in a humidified incubator at 37°C, atmospheric oxygen supplemented with 5% CO_2. Spheroids were allowed to establish for

8 days on ultra-low attaching plates. 96 well U-bottom plates were coated with a solution of 12mg/ml poly-2-hydroxyethyl methacrylate (poly-HEMA (sigma)) dissolved in 95% ethanol. 150 μl of sterile poly-HEMA per well was allowed to evaporate in a sterile biosafety cabinet, dried plates were washed with PBS and stored at 4°C before use. Sub-confluent cultures of B16-F10-OVA were dissociated into single cell suspensions by incubation with accutase for 5 minutes at 37°C and resuspension in growth media. Cells were resuspended at 50.000 cells/ml and plated at 200 μl per well. Cells were concentrated at the bottom of the non-attaching wells by low speed centrifugation at 100 × g for 10 mins. Effector T cells were added after the spheroid media was removed by aspiration, and co-cultures were performed in T cell expansion medium as described above.

Virus generation and transduction

Cyto-roGFP and matrix-roGFP were a gift from Paul Schumacker (Addgene plasmid # 49435 and # 49437). roGFP coding sequences were transferred to an MSCV backbone (MIGR1, addgene plasmid #27490, digested with Bglll and Sall to remove the IRES-GFP cassette) and packaged into ecotropic virus using 293T cells as previously described [47]. $CD8^+$ T cells were isolated and activated as above and after 36 hours, roGFP expressing MSCV-γ retrovirus containing supernatant was added to the cultures in the presence of polybrene (8μg/ml) followed by a 90-minute spin at 30°C at 1000 × G to enhance transduction efficiency. To maintain sensitivity to small changes in redox, cells were infected at an MOI of 1, to achieve low level roGFP expression.

Flow cytometry

Fluorochrome-conjugate monoclonal antibodies were purchased from eBioscience, BDBioscience, or Life Technologies. Staining was performed in 1% FBS/PBS for 30 min on ice, dead cells were excluded with the LIVE/DEAD Fixable Blue Dead Cell Stain Kit (Thermo scientific). Donor-derived CD8+ T cells from blood were quantified after bed blood cell lysis, by direct staining for CD90.1 and CD90.2 congenic markers. For intracellular cytokine staining cells were reactivated with phorbol 12-myristate 13-acetate (PMA, 50ng/ml, Sigma) and ionomycin (500ng/ml, Sigma), in the presence of Brefeldin A (0.1%, Biolegend) for 5 hours prior to fixation using Cytofix Cytoperm (BDBioscience), except for the spheroid cocultures, there Brefeldin was added directly into the coculture (without extra restimulation) 5 hours before staining. For analysis of redox status cells in cell expressing roGFP, the excitation with a 488 nm laser and a 405 nm laser (detection using a was used to quantify reduced and oxidized signal, respectively. FlowJo software was used to generate the derived parameter of the two fluorescent signals. For dynamic assessment of changes in redox state signals were collected for 5 minutes after adding 10mM glucose on an LSRII flow cytometer while the samples were kept at 37°C. The data was plotted as dynamic data after splitting signals into 1 second bins over the full 5-minute period, deriving the mean of the two signals per bin. The gating strategy is shown in the Supplementary Information.

Western blotting

For western blot analysis cells were washed with ice cold PBS and lysed in lysis buffer (20 mM Tris-HCl, [pH 7.5], 150 mM NaCl, 1 mM Na2EDTA, 1 mM EGTA, 1% Triton

X-100, 2.5 mM sodium pyrophosphate, 1 mM β-glycerophosphate, 1 mM Na3VO4, 1 μg/mL leupeptin (Cell Signaling Technologies) supplemented with 1 mM PMSF. Samples were frozen and thawed 3 times followed by centrifugation at 20000g for 10 min at +4° C. Cleared protein lysate was denatured with LDS loading buffer for 10 min at 70° C, and loaded on precast 4% to 12% bis-tris protein gels (Life Technologies). Proteins were transferred onto nitrocellulose membranes using the iBLOT 2 system (Life Technologies) following the manufacturer's protocols. Membranes were blocked with 5% w/v milk and 0.1% Tween-20 in TBS and incubated with the appropriate antibodies in 5% w/v BSA in TBS with 0.1% Tween-20 overnight at 4°C (primary antibodies were at 1:2000 unless otherwise stated below). The following antibodies were used: anti-phospho-ACC1^{Ser79} (cell signaling catalogue #11818); anti-ACC1 (cell signaling catalogue #3676); anti-phospho-AMPK^{Thr172} (Cell Signaling catalogue #2535); anti-AMPK (Cell Signaling catalogue #5831), anti-phospho-S6$^{Ser235/236}$ (cell signaling catalogue #2211); anti-S6 (cell signaling catalogue #2317); anti-phospho-4E-BP1$^{Thr37/45}$ (cell signaling catalogue #2855, at 1:4000); anti-4E-BP1 (cell signaling catalogue #9644, at 1:4000); anti-Glut1 (cell signaling catalogue #12939); and anti-tubulin (Sigma catalogue #T6199, at 1:5000). All primary antibody incubations were followed by incubation with secondary HRP-conjugated antibody (Pierce) in 5% milk and 0.1% Tween-20 in TBS (at 1:20000) and visualized on radiosensitive film (Amersham) using chemiluminescent substrate (Supersignal west-pico, Pierce). Relative optical density was measured using Image J software, and plotted as relative phospho/total protein amount, and as phospho signal optical density.

Single cell RNA sequencing

Single cell RNA sequencing was performed using a 10X Genomics Chromium Controller. OT-I T_E were generated as before and exposed to control or TGR for 20 hours. Single cells were processed with GemCode Single Cell Platform using GemCode Gel Beads, Chip and Library Kits (v2) following the manufacturer's protocol. An estimated 5,000 cells were added to each channel with an average of 3,000 cells recovered. Libraries were sequenced on HiSeq 3000 (Illumina). Samples were demultiplexed and aligned using Cell Ranger 2.2 (10X genomics) then processed and analyzed in R using Seurat [48] and Uniform Manifold Approximation and Projection (UMAP) as a dimensionality reduction approach [49]. Genes from specific metabolic pathways were retrieved from Kegg [50] and expression scores were calculated using Seurat. Differentially expressed genes, with greater than a 1.2 fold change and an adjusted p value of less than 0.1, were analyzed for pathway enrichment using STRING [51].

In vivo tumor experiments

Congenically marked female C57Bl/6 mice (Thy1.1) were shaved, and injected subcutaneously into the right flank of mice with 1 $\times 10^6$ E.G7-OVA in 100μl PBS. After 8 days, donor cells from 3 female mice were mixed before injection and 3 $\times 10^6$ OT-I$^+$ T_E were injected intravenously per tumor bearing mouse, during which the investigator injecting the mice was blinded to the identity of the donor T_E. 3 $\times$ 10^6 OT-I T_E, Right before injection, the size of tumors was measured and equally distributed over both groups (average size was 7mm diameter at D8 in all mice). The grouping of the donor cells was blinded to the investigator injecting the cells, and tumor volumes were measured with calipers every 2

days after T cell infusion, by 2 investigators, one of which was blinded to the identity of the donor cells, to ensure reproducible, unbiased measurements. A small quantity of blood was obtained by facial vein laceration at indicated time points to quantify congenically marked CD8+ T cells by flow cytometry. Congenically marked female C57BL/6 mice (CD45.1) were shaved, and injected subcutaneously into the right flank of mice with 1×10^6 B16-OVA cells in 100 μl PBS. Tumor growth was monitored every 2 days by measuring the diameter of the tumor mass. After 5 days, 5×10^6 OT-I T_E that had previously been activated in vitro with SIINFELK peptide, were transferred i.v. into tumor bearing mice. Control groups did not receive T_E injection. The grouping of the donor cells was blinded to the investigator injecting the cells. On day 3, 6 and 9 after tumor inoculation, mice were treated with an intraperitoneal injection of 200 μg anti-PD-1 antibody or IgG2a isotype control in 100 μl PBS. On day 21 after tumor inoculation, mice were humanely euthanized and the tumor mass was excised. Isolated tumors were homogenized to obtain single cell suspensions and analyzed by flow cytometry

Statistics

Statistical analysis was performed using prism 8 software (Graph pad) and results are represented as mean ± SEM, unless otherwise indicated. Comparisons for two groups were calculated using unpaired two-tailed Student's *t* tests, comparisons of more than two groups were calculated using an Ordinary one-way ANOVA with Bonferroni's multiple comparison tests or 2way ANOVA with Bonferroni's multiple comparison tests. We observed normal distribution and no difference in variance between groups in individual comparisons. Selection of sample size was based on extensive experience with metabolic and *in vivo* tumor immunology assays. Also see Reporting Summary.

Data Availability

The data that support the findings of this study are available from the corresponding author upon request. Single cell RNA sequencing data has been deposited in the Gene Ontology Omnibus under accession number GSE152018.

Extended Data

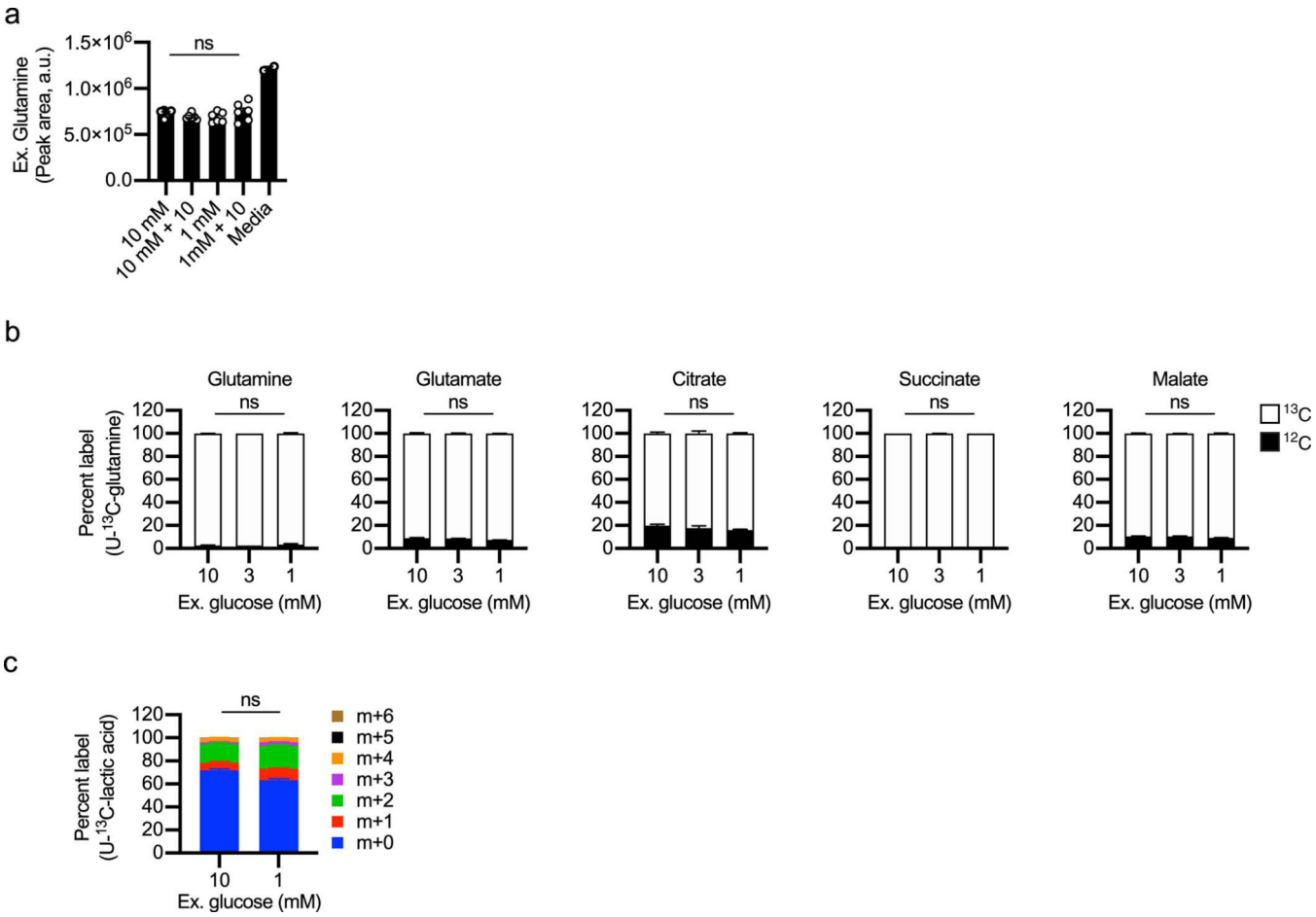

Extended Data Fig. 1. TGR CD8$^+$ T_E do not sustain mitochondrial metabolism by incorporating more glutamine-derived carbons into the TCA cycle.

WT CD8$^+$ T cells isolated from spleens of C7BI/6 mice were activated with anti-CD3 (5 mg/mL), anti-CD28 (0.5 mg/mL), IL-2 (100 U/mL), expanded for a total of 72 hours, and exposed to 10mM, 3mM, or 1mM glucose as indicated in cultures set to 1 million per ml. (**a**) Polar metabolites were extracted from 500µl media supernatant from 20h cultures of 10mM and 1mM cells. Bar graphs represent glutamine concentration in unused culture media for n=3 biological replicates. Significance was calculated using 2-tailed Student's *t* tests, no significant changes (ns) were observed. (**b**) T_E were generated as above, but during the final 20h all groups were cultured in 4mM heavy labeled (U-^{13}C) glutamine (100% U-^{13}C glutamine). Polar metabolites were extracted and isotopologue distribution assessed by targeted mass spectrometry. TCA intermediates are plotted as percent label from newly metabolized U-^{13}C (open bars) or remaining U-^{12}C (black bars) glutamine carbons. Data are from n=3 biological replicates, representative of 2 independent experiments. Significance was calculated using 2-tailed Student's *t* tests, no significant changes were observed. (**c**) T_E were generated as above, but during the final 6h 2mM U-^{13}C-lactate was added to the culture. Polar metabolites were extracted and isotopologue distribution assessed by targeted mass spectrometry. Significance was calculated using 2-tailed Student's *t* tests

comparing the predominant m+2 isotopologue group in both conditions. Data shown for n=3 biological replicates. Significance was calculated using 2-tailed Student's *t* tests, No significant changes were observed. All error bars show SEM.

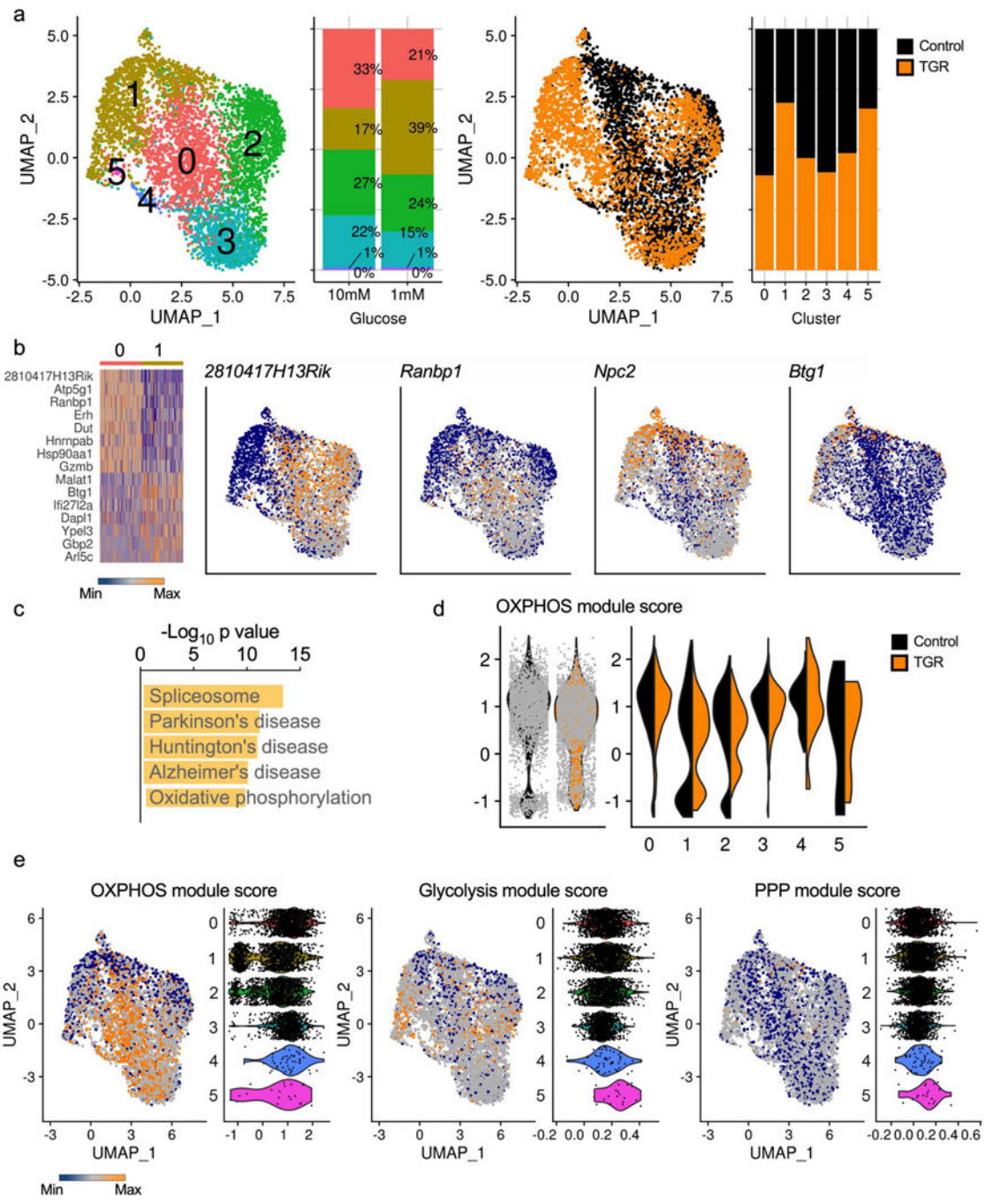

Extended Data Fig. 2. Limited transcriptional reprogramming during TGR.

WT CD8$^+$ T cells isolated from spleens of C7Bl/6 mice were activated with anti-CD3 (5 mg/mL), anti-CD28 (0.5 mg/mL), IL-2 (100 U/mL), expanded for a total of 72 hours, and exposed to 10mM (black) or 1mM (orange) glucose in cultures set to 1 million per ml. RNA

isolated from single cells was sequenced using the 10X genomics platform and analyzed to explore transcriptional changes in each population of cells. **(a)** A Uniform Manifold Approximation and Projection (UMAP) of the overlapped cells from each treatment (control, black; TGR, orange), clustered on the basis of transcriptional similarity is shown highlighting clusters and treatment distribution. Bar graphs depicting cluster distribution for each condition are also shown. **(b)** Clusters 0 and 1, where least overlap between treatments was observed, were contrasted to look for differentially expressed genes (> 1.2-fold change and < 0.1 adjusted p-value); a heatmap of top up and down regulated genes is shown, along with UMAPs of example genes. (**c**) The top 5 most enriched pathways in differentially regulated genes between cluster 0 and 1. (**d**) Module scores based on average expression levels of gene programs were calculated for 18 differentially expressed OXPHOS genes (*Atp5g1*, *Atp5g3*, *Cox5a*, *Cox6a1*, *Cyc1*, *Ndufa11*, *Ndufa12*, *Ndufa4*, *Ndufa8*, *Ndufabl*, *Ndufb7*, *Ndufb8*, *Ndufcl*, *Ndufc2*, *Ndufs6*, *Sdhb*, *Uqcr10*, *Uqcr11*). Violin plots depict the global OXPHOS module score per condition (left) or per cluster and condition (right). (**e**) Module scores based on average expression levels of gene programs were also calculated for enzyme-coding genes involved in glycolysis (mmu00010) or the pentose phosphate pathway (PPP, mmu00030) based on Kegg annotation. UMAP and Violin plots illustrate the OXPHOS, glycolysis and PPP modules, with the violin plots divided per cluster.

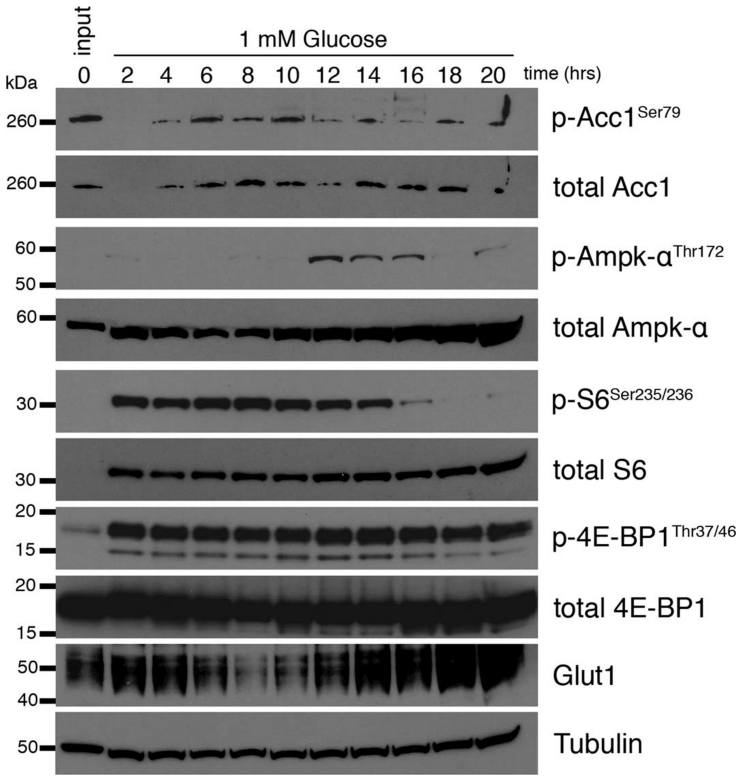

Extended Data Fig. 3. Signaling timecourse during TGR

Protein isolates were prepared as described in (figure 3f), taking samples every 2h over the 20h exposure to limiting glucose concentration. Immunoblot analysis of protein extracts from equal cell numbers probed for phosphorylated acetyl-coA carboxylase at Ser79 (p-ACC1^{Thr79}), total ACC1, phosphorylated AMPK at Thr172 (p-AMPk^{Thr172}),

total AMPK, phosphorylated ribosomal protein S6 at Ser235/236 (p-S6$^{Ser235/236}$), total S6, phosphorylated 4E-binding protein 1 at Thr37/46 (p-4E-BP1$^{Thr37/46}$), total 4E-BP1, and Glut1. Tubulin was used as a loading control. Optical density was measured and changes in phosphorylation are shown relative to total protein and as direct measurements. Representative of 3 biological independent samples. Biological replicate data is shown in Fig. 3f.

a

XCMS analysis of total pools followed by Kegg pathways search

Increased in 1mM refed

ID	Pathway	#metabolites
hsa01100	Metabolic pathways	38
hsa00520	Amino sugar and nucleotide sugar metabolism	8
hsa01200	Carbon metabolism	8
hsa00051	Fructose and mannose metabolism	7
hsa00562	Inositol phosphate metabolism	7
hsa00230	Purine metabolism	7
hsa00240	Pyrimidine metabolism	6
hsa00030	Pentose phosphate pathway	6
hsa04070	Phosphatidylinositol signaling system	6
hsa01230	Biosynthesis of amino acids	6
hsa05230	Central carbon metabolism in cancer	5

Decreased in 1mM refed

ID	Pathway	#metabolites
hsa01100	Metabolic pathways	20
hsa01230	Biosynthesis of amino acids	5
hsa01210	2-Oxocarboxylic acid metabolism	3
hsa01200	Carbon metabolism	3
hsa05230	Central carbon metabolism	3
hsa04070	Phosphatidylinositol signaling system	3
hsa00330	Arginine and proline metabolism	3
hsa00562	Inositol phosphate metabolism	3
hsa04723	Retrograde endocannabanoid signalling	2
hsa04730	Long-term depression	2
hsa04720	Long-term potentiation	2

b

X13CMS analysis of isotope incorporation followed by Kegg pathways search

Increased in 1mM refed

ID	Pathway	#metabolites
hsa01100	Metabolic pathways	36
hsa01200	Carbon metabolism	9
hsa01210	2-Oxocarboxylic acid metabolism	7
hsa00030	Pentose phosphate pathway	5
hsa05230	Central carbon metabolism in cancer	4
hsa04922	Glucagon signaling pathway	4
hsa00040	Pentose and glucuronate interconversions	4
hsa04070	Phosphatidylinositol signaling system	4
hsa00020	Citrate cycle (TCA cycle)	3
hsa00750	Vitamin B6 metabolism	3
hsa00240	Pyrimidine metabolism	3

c

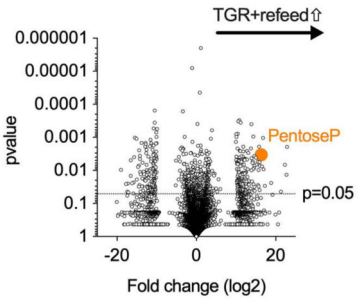

Extended Data Fig. 4. TGR T_E have altered glucose reallocation upon re-exposure to drive anabolic metabolism.

WT CD8$^+$ T cells isolated from spleens of C7Bl/6 mice were activated with anti-CD3 (5 mg/mL), anti-CD28 (0.5 mg/mL), IL-2 (100 U/mL), expanded for a total of 72 hours, and exposed to 10mM (control) or 1mM (TGR) glucose during the final 5 minutes cells were re-exposed to normal (U-^{12}C) glucose or heavy labeled (U-^{13}C) glucose. 20h cultures were started at 1×10^6 (control) and 1.5×10^6 (TGR) cells per/ml to generate similar end concentrations for glucose pulse experiments. (**a**) Table showing the results of a Kegg-pathway analysis of the significantly increased and decreased metabolite pools in TGR T_E after normal (U-^{12}C) glucose re-feeding when compared to re-fed control T_E. (**b**) Table shows the results of a Kegg pathway analysis of the metabolites that exhibited increased glucose-derived U-^{13}C assimilation (as determined by X13CMS software) after re-feeding TGR T_E with heavy labeled (U-^{13}C) glucose compared to re-fed control T_E. Data are from 3 biological replicates, representative of 3 independent experiments. Kegg Pathways were ranked according to the number of metabolite hits in that pathway (from highest to lowest). Metabolites in the highest ranked pathways were further validated by targeted analysis. (**c**) Polar metabolites were extracted and untargeted metabolomic analysis was performed using XCMS on cells re-exposed to normal (U-^{12}C) glucose. Volcano plot depicts relative metabolite pools compared between control and TGR cells. Orange circle represents a pentose phosphate pathway metabolite Pentose-phosphate, significantly increased in glucose re-fed TGR T_E. Statistical significance was calculated using a Welch's t-test, comparing relative intensities of each isotopologue in labeled samples of control T_E versus those of TGR T_E.

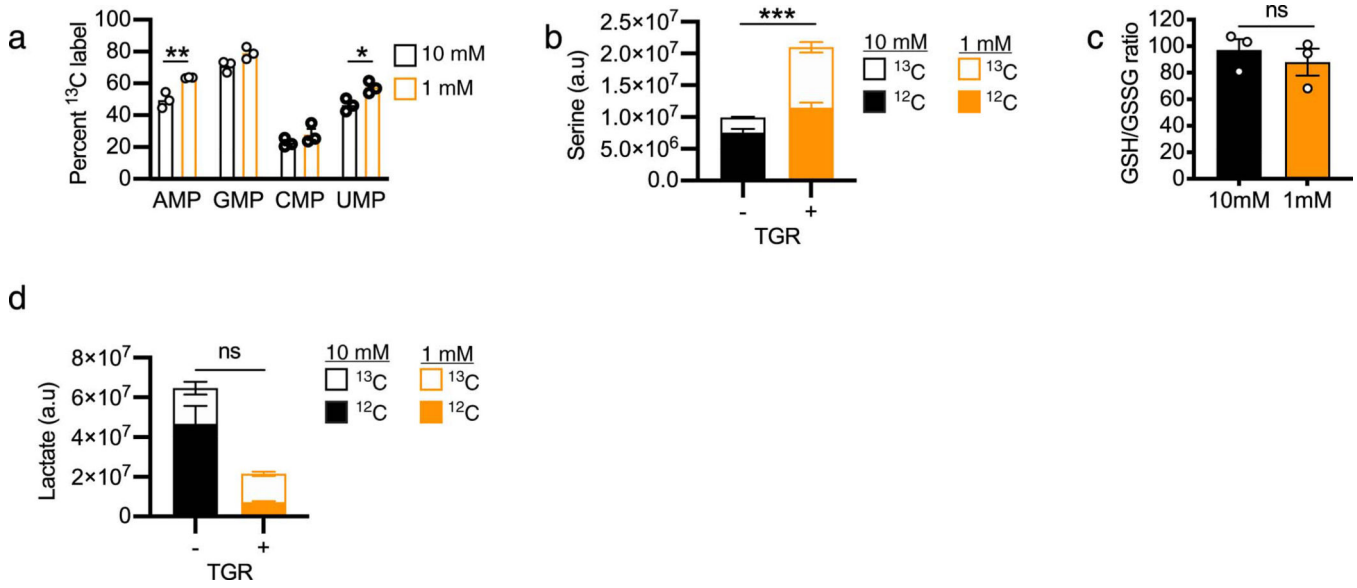

Extended Data Fig. 5. 6h U-^{13}C-glucose re-exposure following TGR.

WT CD8$^+$ T cells isolated from spleens of C7Bl/6 mice were activated with anti-CD3 (5 mg/mL), anti-CD28 (0.5 mg/mL), IL-2 (100 U/mL), expanded for a total of 72 hours, and exposed to 10mM (black) or 1mM (orange) glucose. Cells were re-exposed to 10mM U-13C-glucose for 6h prior to polar metabolite extraction and analysis by LC-MS. 20h cultures were started at 1×10^6 (control) and 1.5×10^6 (TGR) cells per/ml to generate similar end concentrations for glucose pulse experiments. (**a**) Percent ^{13}C label incorporation

into nucleotide monophosphates was analyzed. Data are from n=3 biological replicates. Significance was calculated using 2-tailed Student's *t* tests. * p<0.05. (**b**) Relative ^{13}C label incorporation into serine was analyzed. Data are from n=3 biological replicates. Significance was calculated using 2way ANOVA. Significance is indicated for the ^{13}C portion (open bars). *** p<0.001. The ^{12}C portion (filled bars) was also significant. ** p<0.01. (**c**) The GSH/GSSG ratio was calculated from summed isotopologues for each metabolite. Data are from n=3 biological replicates. Significance was calculated using 2-tailed Student's *t* tests, no significant difference was found. (**d**) Relative ^{13}C label incorporation into lactate was analyzed. Data are from n=3 biological replicates. Significance was calculated using 2way ANOVA. Significance is indicated for the ^{13}C portion (open bars), which was not significant. The ^{12}C portion (filled bars) was significant. *** p<0.001. All error bars show SEM.

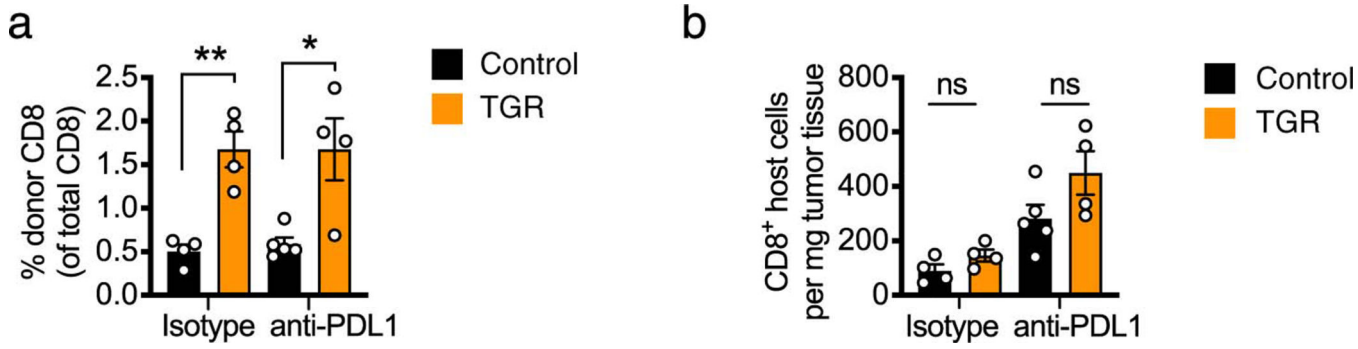

Extended Data Fig. 6. TGR enhances CD8$^+$ tumour-specific antitumour function *in vivo*.
As depicted in Fig. 6f, CD45.1 female recipient mice were injected subcutaneously with 1×10^6 B16-OVA melanoma cells and tumors established for 5 days. 5×10^6 control (black) or TGR (orange) OT-I$^+$ T_E were injected intravenously per tumor bearing mouse. Mice receiving no T_E were used as control. 3, 6 and 9 days after tumor inoculation, mice received 200 μg anti-PD-1 antibody or IgG2a isotype control in 100 μl PBS intraperitoneally. (**a**) 21 days after tumor inoculation mice were humanely euthanized, blood was collected, red cells were lysed, and the white blood cell fraction stained for congenic markers. Data are presented as % of donor-derived (CD45.2$^+$) CD8$^+$ T cells as a fraction to total circulating CD8$^+$ T cells and each dot represents an individual mouse (n=5). Statistical significance was calculated by 2-tailed Student's *t* test. * p<0.05; ** p<0.01. (**b**) 21 days after tumor inoculation mice were humanely euthanized and the tumor mass was excised. Single cell suspensions were analyzed by flow cytometry. The number of host (CD45.1) CD8$^+$ T cells per mg tissue was quantified and each dot represents an individual mouse (n=5). Statistical significance was calculated by 2-tailed Student's *t* test. ns not significant. All error bars show SEM.

Supplementary Material

Refer to Web version on PubMed Central for supplementary material.

Acknowledgements

We thank members of the Pearce laboratories for support and helpful discussions and Andrea Quintana, and John Sutherland mouse colony management. This work was funded by the NIH (CA181125 to E.L.P. and AI110481 to E.J.P.), and the Max Planck Society. R.Z. was supported by the DFG (SFB1160, B09, TRR167, B06) and ERC (GVHD Cure n° 681012).

References

1. Michalek RD et al. in J Immunol Vol. 186 3299–3303 (American Association of Immunologists, 2011). [PubMed: 21317389]
2. Maciver NJ et al. in J. Leukoc. Biol Vol. 84 949–957 (Society for Leukocyte Biology, 2008). [PubMed: 18577716]
3. Chang C-H et al. in Cell Vol. 162 1229–1241 (2015). [PubMed: 26321679]
4. Chang C-H et al. in Cell Vol. 153 1239–1251 (2013). [PubMed: 23746840]
5. Blagih J. et al. The energy sensor AMPK regulates T cell metabolic adaptation and effector responses in vivo. Immunity 42, 41–54, doi:10.1016/j.immuni.2014.12.030 (2015). [PubMed: 25607458]
6. Rolf J. et al. AMPKalpha1: a glucose sensor that controls CD8 T-cell memory. Eur J Immunol 43, 889–896, doi:10.1002/eji.201243008 (2013). [PubMed: 23310952]
7. Klein Geltink RI et al. Mitochondrial Priming by Cd28. Cell 171, 385–397 e311, doi:10.1016/j.cell.2017.08.018 (2017). [PubMed: 28919076]
8. Buck MD et al. Mitochondrial Dynamics Controls T Cell Fate through Metabolic Programming. Cell 166, 63–76, doi:10.1016/j.cell.2016.05.035 (2016). [PubMed: 27293185]
9. Sukumar M. et al. Inhibiting glycolytic metabolism enhances CD8+ T cell memory and antitumor function. J Clin Invest 123, 4479–4488, doi:10.1172/JCI69589 (2013). [PubMed: 24091329]
10. Sukumar M. et al. in Cell Metabolism Vol. 23 63–76 (2016). [PubMed: 26674251]
11. Scharping NE et al. in Immunity Vol. 45 374–388 (2016). [PubMed: 27496732]
12. Chowdhury PS, Chamoto K, Kumar A. & Honjo T. PPAR-Induced Fatty Acid Oxidation in T Cells Increases the Number of Tumor-Reactive CD8. Cancer Immunol Res 6, 1375–1387, doi:10.1158/2326-6066.CIR-18-0095 (2018). [PubMed: 30143538]
13. Buck MD, Sowell RT, Kaech SM & Pearce EL in Cell Vol. 169 570–586 (2017). [PubMed: 28475890]
14. Qiu J. et al. Acetate Promotes T Cell Effector Function during Glucose Restriction. Cell Rep 27, 2063–2074.e2065, doi:10.1016/j.celrep.2019.04.022 (2019). [PubMed: 31091446]
15. Crompton JG, Sukumar M. & Restifo NP Targeting Akt in cell transfer immunotherapy for cancer. Oncoimmunology 5, e1014776, doi:10.1080/2162402X.2015.1014776 (2016).
16. Nabe S. et al. Reinforce the antitumor activity of CD8. Cancer Sci 109, 3737–3750, doi:10.1111/cas.13827 (2018). [PubMed: 30302856]
17. Hosios AM et al. in Dev. Cell Vol. 36 540–549 (2016). [PubMed: 26954548]
18. Garcia D. & Shaw RJ AMPK: Mechanisms of Cellular Energy Sensing and Restoration of Metabolic Balance. Mol Cell 66, 789–800, doi:10.1016/j.molcel.2017.05.032 (2017). [PubMed: 28622524]
19. Jacobs SR et al. in J Immunol Vol. 180 4476–4486 (American Association of Immunologists, 2008). [PubMed: 18354169]
20. Macintyre AN et al. in Cell Metabolism Vol. 20 61–72 (2014). [PubMed: 24930970]
21. Siska PJ et al. in J Immunol Vol. 197 2532–2540 (American Association of Immunologists, 2016). [PubMed: 27511728]
22. Saxton RA & Sabatini DM in Cell Vol. 168 960–976 (2017). [PubMed: 28283069]
23. Waypa GB et al. Hypoxia triggers subcellular compartmental redox signaling in vascular smooth muscle cells. Circ Res 106, 526–535, doi:10.1161/CIRCRESAHA.109.206334 (2010). [PubMed: 20019331]

24. Schieber M. & Chandel NS ROS function in redox signaling and oxidative stress. Curr Biol 24, R453–462, doi:10.1016/j.cub.2014.03.034 (2014). [PubMed: 24845678]
25. Hosios AM & Vander Heiden MG The redox requirements of proliferating mammalian cells. J Biol Chem 293, 7490–7498, doi:10.1074/jbc.TM117.000239 (2018). [PubMed: 29339555]
26. Kong H. & Chandel NS Regulation of redox balance in cancer and T cells. J Biol Chem 293, 7499–7507, doi:10.1074/jbc.TM117.000257 (2018). [PubMed: 29282291]
27. Mak TW et al. in Immunity Vol. 46 675–689 (2017). [PubMed: 28423341]
28. Smith CA, Want EJ, O'Maille G, Abagyan R. & Siuzdak G. XCMS: processing mass spectrometry data for metabolite profiling using nonlinear peak alignment, matching, and identification. Anal Chem 78, 779–787, doi:10.1021/ac051437y (2006). [PubMed: 16448051]
29. Huang X. et al. X13CMS: global tracking of isotopic labels in untargeted metabolomics. Anal Chem 86, 1632–1639, doi:10.1021/ac403384n (2014). [PubMed: 24397582]
30. Ma EH et al. in Cell Metab. Vol. 25 345–357 (2017). [PubMed: 28111214]
31. Crompton JG et al. Akt inhibition enhances expansion of potent tumor-specific lymphocytes with memory cell characteristics. Cancer Res 75, 296–305, doi:10.1158/0008-5472.CAN-14-2277 (2015). [PubMed: 25432172]
32. Vander Heiden MG, Cantley LC & Thompson CB Understanding the Warburg effect: the metabolic requirements of cell proliferation. Science 324, 1029–1033, doi:10.1126/science.1160809 (2009). [PubMed: 19460998]
33. Warburg O. in The Journal of Cancer Research Vol. 9 148–163 (American Association for Cancer Research Journals, 1925).
34. Liberti MV & Locasale JW in Trends Biochem. Sci Vol. 41 211–218 (2016). [PubMed: 26778478]
35. Zhao J, Song Y. & Liu D. Clinical trials of dual-target CAR T cells, donor-derived CAR T cells, and universal CAR T cells for acute lymphoid leukemia. J Hematol Oncol 12, 17, doi:10.1186/s13045-019-0705-x (2019). [PubMed: 30764841]
36. Sena LA et al. in Immunity Vol. 38 225–236 (2013). [PubMed: 23415911]
37. Nathan C. & Cunningham-Bussel A. Beyond oxidative stress: an immunologist's guide to reactive oxygen species. Nat Rev Immunol 13, 349–361, doi:10.1038/nri3423 (2013). [PubMed: 23618831]
38. Chatterjee S. et al. CD38-NAD +Axis Regulates Immunotherapeutic Anti-Tumor T Cell Response. Cell Metab 27, 85–100.e108, doi:10.1016/j.cmet.2017.10.006 (2018). [PubMed: 29129787]
39. Johnson MO et al. Distinct Regulation of Th17 and Th1 Cell Differentiation by Glutaminase-Dependent Metabolism. Cell 175, 1780–1795.e1719, doi:10.1016/j.cell.2018.10.001 (2018). [PubMed: 30392958]
40. Ghergurovich JM et al. A small molecule G6PD inhibitor reveals immune dependence on pentose phosphate pathway. Nat Chem Biol, doi:10.1038/s41589-020-0533-x (2020).
41. Ma EH et al. Metabolic Profiling Using Stable Isotope Tracing Reveals Distinct Patterns of Glucose Utilization by Physiologically Activated CD8. Immunity 51, 856–870.e855, doi:10.1016/j.immuni.2019.09.003 (2019). [PubMed: 31747582]
42. Yang JC & Rosenberg SA Adoptive T-Cell Therapy for Cancer. Adv Immunol 130, 279–294, doi:10.1016/bs.ai.2015.12.006 (2016). [PubMed: 26923004]
43. Chamoto K. et al. Mitochondrial activation chemicals synergize with surface receptor PD-1 blockade for T cell-dependent antitumor activity. Proc Natl Acad Sci U S A 114, E761–E770, doi:10.1073/pnas.1620433114 (2017). [PubMed: 28096382]
44. Kumar A, Chamoto K, Chowdhury PS & Honjo T. Tumors attenuating the mitochondrial activity in T cells escape from PD-1 blockade therapy. Elife 9, doi:10.7554/eLife.52330 (2020).

Methods-only References

45. Wills J, Edwards-Hicks J. & Finch AJ AssayR: A Simple Mass Spectrometry Software Tool for Targeted Metabolic and Stable Isotope Tracer Analyses. Anal Chem 89, 9616–9619, doi:10.1021/acs.analchem.7b02401 (2017). [PubMed: 28850215]

46. van der Windt GJW, Chang CH & Pearce EL Measuring Bioenergetics in T Cells Using a Seahorse Extracellular Flux Analyzer. Curr Protoc Immunol 113, 3.16B.11–13.16B.14, doi:10.1002/0471142735.im0316bs113 (2016).

47. Pearce EL et al. in Nature Vol. 460 103–107 (2009). [PubMed: 19494812]

48. Butler A, Hoffman P, Smibert P, Papalexi E. & Satija R. Integrating single-cell transcriptomic data across different conditions, technologies, and species. Nat Biotechnol 36, 411–420, doi:10.1038/nbt.4096 (2018). [PubMed: 29608179]

49. Diaz-Papkovich A, Anderson-Trocme L, Ben-Eghan C. & Gravel S. UMAP reveals cryptic population structure and phenotype heterogeneity in large genomic cohorts. PLoS Genet 15, e1008432, doi:10.1371/journal.pgen.1008432 (2019).

50. Aoki-Kinoshita KF & Kanehisa M. Gene annotation and pathway mapping in KEGG. Methods Mol Biol 396, 71–91, doi:10.1007/978-1-59745-515-2_6 (2007). [PubMed: 18025687]

51. Szklarczyk D. et al. STRING v11: protein-protein association networks with increased coverage, supporting functional discovery in genome-wide experimental datasets. Nucleic Acids Res 47, D607–D613, doi:10.1093/nar/gky1131 (2019). [PubMed: 30476243]

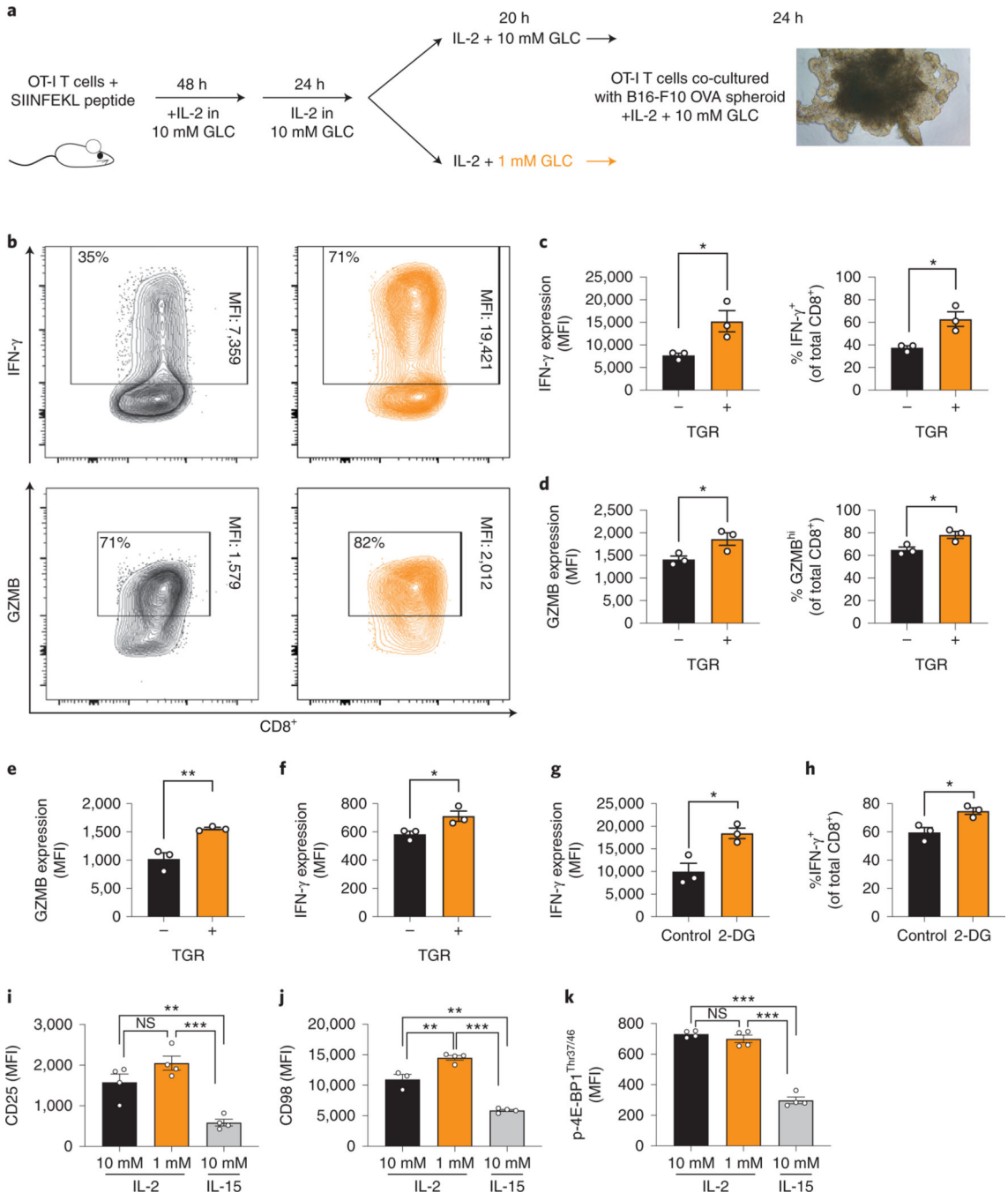

Fig. 1. TGR enhances CD8$^+$ T_E effector molecule expression upon glucose re-exposure.

(**a**) To generate OVA-specific CD8$^+$ T_E, OT-I splenocytes were activated with SIINFEKL peptide and IL-2 (100 U/mL), expanded for 72 hours total, followed by 20 hours of exposure to 10mM (control, black) or 1mM (TGR, orange) glucose in cultures set to 1 million per ml. B16-F10-OVA cells were established as multicellular spheroids for 8 days. (**b**) 100.000 OT-I T_E cells generated as in (**a**) were combined with spheroid cultures in refreshed media containing 10mM glucose and IL-2, co-cultured for 20 hours, treated with brefeldin-A and assessed for intracellular cytokine expression induced by tumor-expressed antigen.

Representative scatter plots are shown. (**c-d**) Quantification of IFN-γ and GZMB per cell (MFI, left) and number of IFN-γ^+ or $GZMB^{hi}$ cells (right). Points represent averaged data from 4 independent co-cultures. data shown for 3 biological replicates. Statistical significance was calculated by 2-tailed Student's *t* test. * p<0.05. (**e-k**) WT $CD8^+$ T cells isolated from spleens of C7Bl/6 mice were activated with anti-CD3 (5 mg/mL), anti-CD28 (0.5 mg/mL), IL-2 (100 U/mL), expanded for a total of 72 hours, to 10mM (control, black) or 1mM (TGR, orange) glucose in cultures set to 1 million per ml. (**e-f**) Cells were restimulated using PMA/ionomycin with brefeldin-A and assessed for intracellular levels of (**e**) GZMB and (**f**) IFN-γ. Data show 3 biological replicates and are representative of 3 independent experiments. Statistical significance was calculated by 2-tailed Student's *t* test. * p<0.05, ** p<0.01. (**g-h**) WT $CD8^+$ T were isolated, activated and expanded as in (e-f), and exposed to 2-deoxy-glucose (2-DG, 0.5mM) for 20h. 2-DG was removed, cell were restimulated as above and assessed for intracellular (**g**) IFN-γ expression and (**h**) number of IFN-γ^+ cells. Data show 3 biological replicates and statistical significance was calculated by 2-tailed Student's *t* test. * p<0.05. (**i-k**) WT $CD8^+$ T cells activated and starved as in (**e,f**) or exposed to 100u IL-15 for 20h. Expression of (**i**) CD25, (**j**) CD98 and (**k**) p-4E-$BP1^{Thr37/46}$ were assessed. Data show n=4 biological replicates. Statistical significance was calculated by 2-tailed Student's *t* test. * p<0.05; ** p<0.01; *** p<0.001. All error bars show SEM.

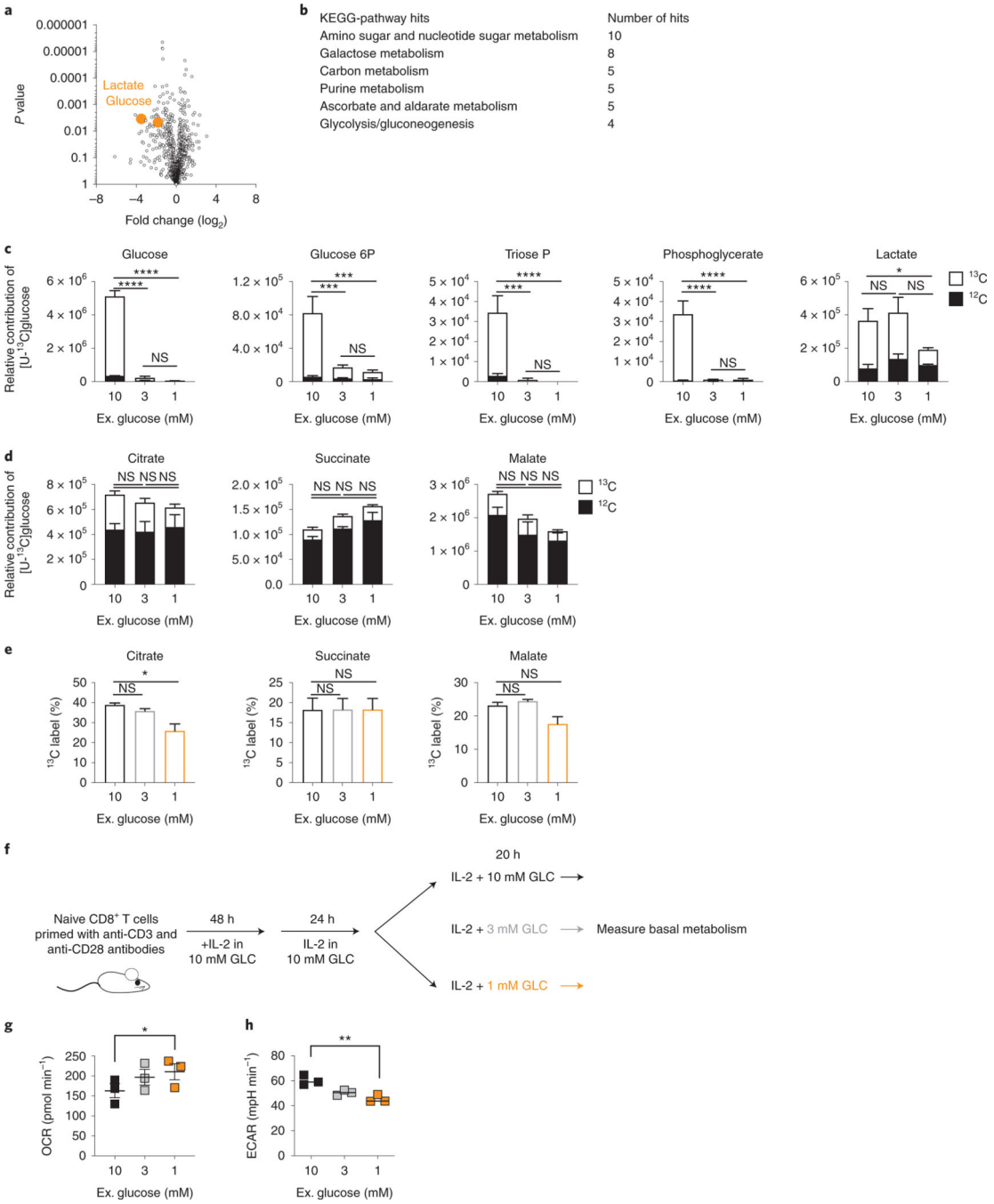

Fig. 2. TGR T_E have depleted sugar metabolism, but sustain TCA cycle metabolites.

WT $CD8^+$ T cells were isolated, activated and expanded as in (Fig. 1e–k), followed by 20h exposure to 10mM, 1mM glucose. in cultures set to 1 million per ml. (**a**) Polar metabolites were extracted followed by untargeted metabolomic analysis. Volcano plot compares relative metabolite pools between control and TGR cells, orange circles represent the first and last metabolites of aerobic glycolysis, significantly reduced in TGR T_E. (**b**) Table showing Kegg-pathway analysis of the significantly reduced metabolites in TGR T_E identified in (**a**). (**c-e**) WT T_E were generated as above, but during the final 20 hours, normal (U-^{12}C)

glucose was exchanged for heavy labeled (U-^{13}C) glucose in the annotated concentrations. Polar metabolites were extracted and isotopologue distribution assessed by targeted mass spectrometry. (**c-d**) Relative contribution to glycolytic intermediates and TCA intermediates respectively. Statistical analysis was carried out on n=3 biological replicates, representative of 3 independent experiments, using a 2way ANOVA. Statistical significance is indicated for the ^{13}C portion (open bars). *p<0.05; **p<0.01; ***p<0.001; ****p<0.0001; ns=not significant. No statistical significance was observed in the ^{12}C portion (filled bars), with the exception of succinate, which significantly increased in 1mM compared to 10mM (p<0.01). (**e**) Percent ^{13}C contribution to TCA intermediates. Statistical analysis was carried out on 3 biological replicates, representative of 3 independent experiments, using an Ordinary one-way ANOVA. *p<0.05; ns=not significant. (**f**) WT CD8^{+} T cells isolated from spleens of C7Bl/6 mice were activated with anti-CD3 (5 mg/mL), anti-CD28 (0.5 mg/mL), IL-2 (100 U/mL), expanded for a total of 72 hours, and exposed to 10mM (black) 3mM (grey) or 1mM (orange) glucose in cultures set to 1 million per ml. (**g-h**) 2 ×10^{5} T cells were plated in triplicate in assay medium containing the indicated concentration of glucose for analysis in a Seahorse extracellular flux analyzer. (**g**) Basal oxygen consumption rate (OCR) and (**h**) extracellular acidification rate (ECAR) were measured 3 times over a span of 20 minutes. Data represent average of n=3 independent biological replicates. Statistical significance was calculated using a 2-tailed Student's *t* test. * p< 0.05; ** p<0.01, data representative of >3 independent experiments. All error bars show SEM.

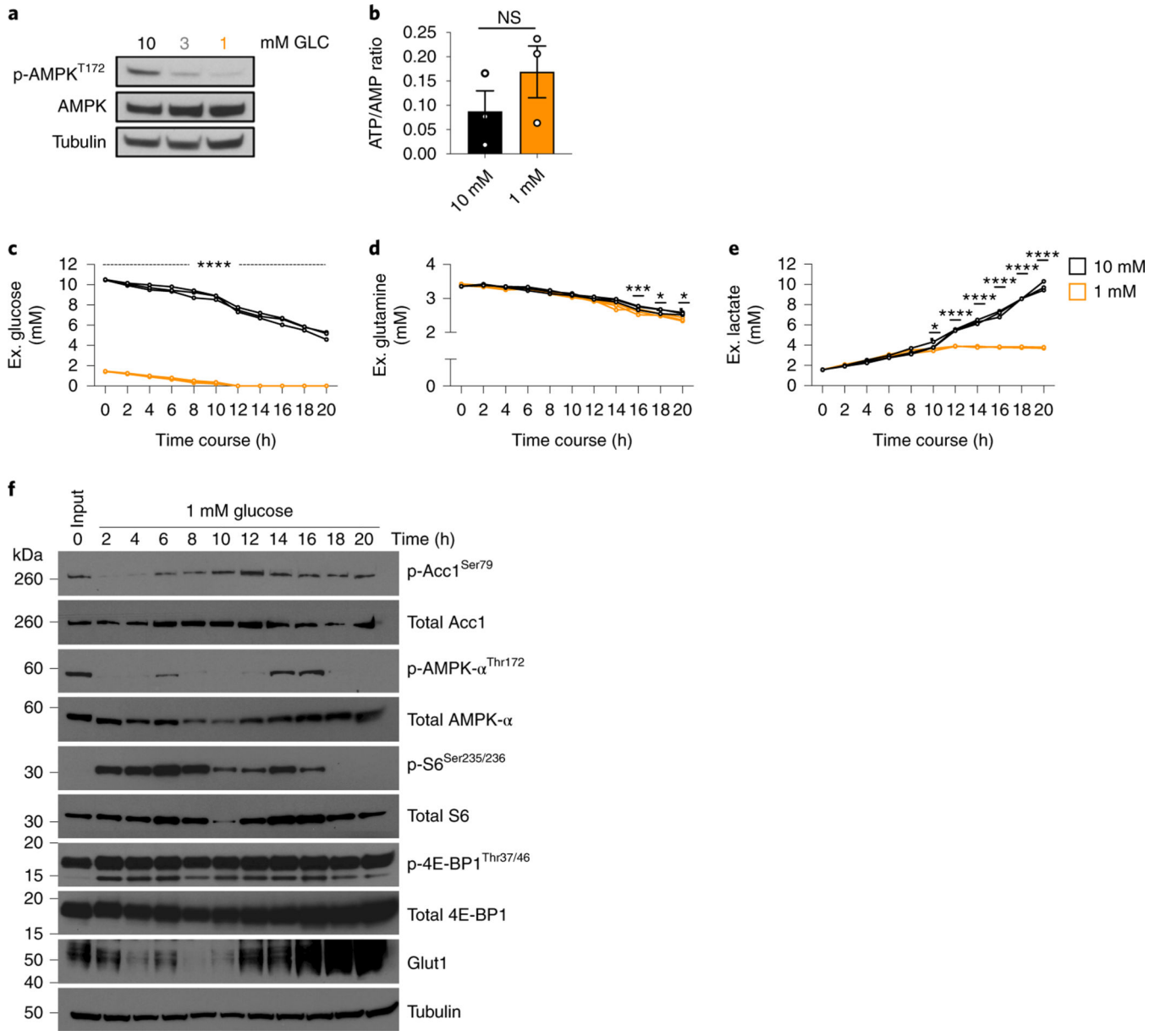

Fig. 3. TGR CD8$^+$ T_E are metabolically active and energetically balanced.

(a-f) WT CD8$^+$ T cells isolated from spleens of C7Bl/6 mice were activated with anti-CD3 (5 mg/mL), anti-CD28 (0.5 mg/mL), IL-2 (100 U/mL), expanded for a total of 72 hours, and exposed to 10mM (black) or 1mM (orange) glucose in cultures set to 1 million per ml. (**a**) Immunoblot analysis of protein extracts from equal cell numbers probed for phosphorylated AMPK at Thr172 (p-AMPk^{Thr172}) and total AMPK. Tubulin was used as a loading control. Data are representative of 3 independent experiments, and 4 biological replicates. (**b**) Polar metabolites were extracted, levels of ATP (a.u.) and AMP (a.u.) were measured by liquid-chromatography mass spectrometry and ratios (a.u.) were calculated for 3 independent biological replicates. No significant differences were observed using a 2-tailed Student's *t* test. Representative of 2 independent experiments. (**c-e**) Media samples and (**f**) protein isolates were collected every 2h over the 20h exposure to limiting glucose

concentrations. Changes in media (**c**) glucose, (**d**) glutamine, and (**e**) lactate concentration were measured over the 20h timecourse using a Cedex Bio Analyzer. Statistical significance was calculated from 3 biological replicates using 2way ANOVA. * $p<0.05$; *** $p<0.001$; ****$p<0.0001$. (**f**) Immunoblot analysis of protein extracts from equal cell numbers probed for phosphorylated acetyl-coA carboxylase at Ser79 (p-ACC1^{Thr79}), total ACC1, phosphorylated AMPK at Thr172 (p-AMPk^{Thr172}), total AMPK, phosphorylated ribosomal protein S6 at Ser235/236 (p-S6$^{Ser235/236}$), total S6, phosphorylated 4E-binding protein 1 at Thr37/46 (p-4E-BP1$^{Thr37/46}$), total 4E-BP1, and Glut1. Tubulin was used as a loading control. Optical density was measured and changes in phosphorylation are shown relative to total protein and as direct measurements. Representative of 3 biological independent samples. Biological replicate data is shown in Extended Data Fig. 3. All error bars show SEM.

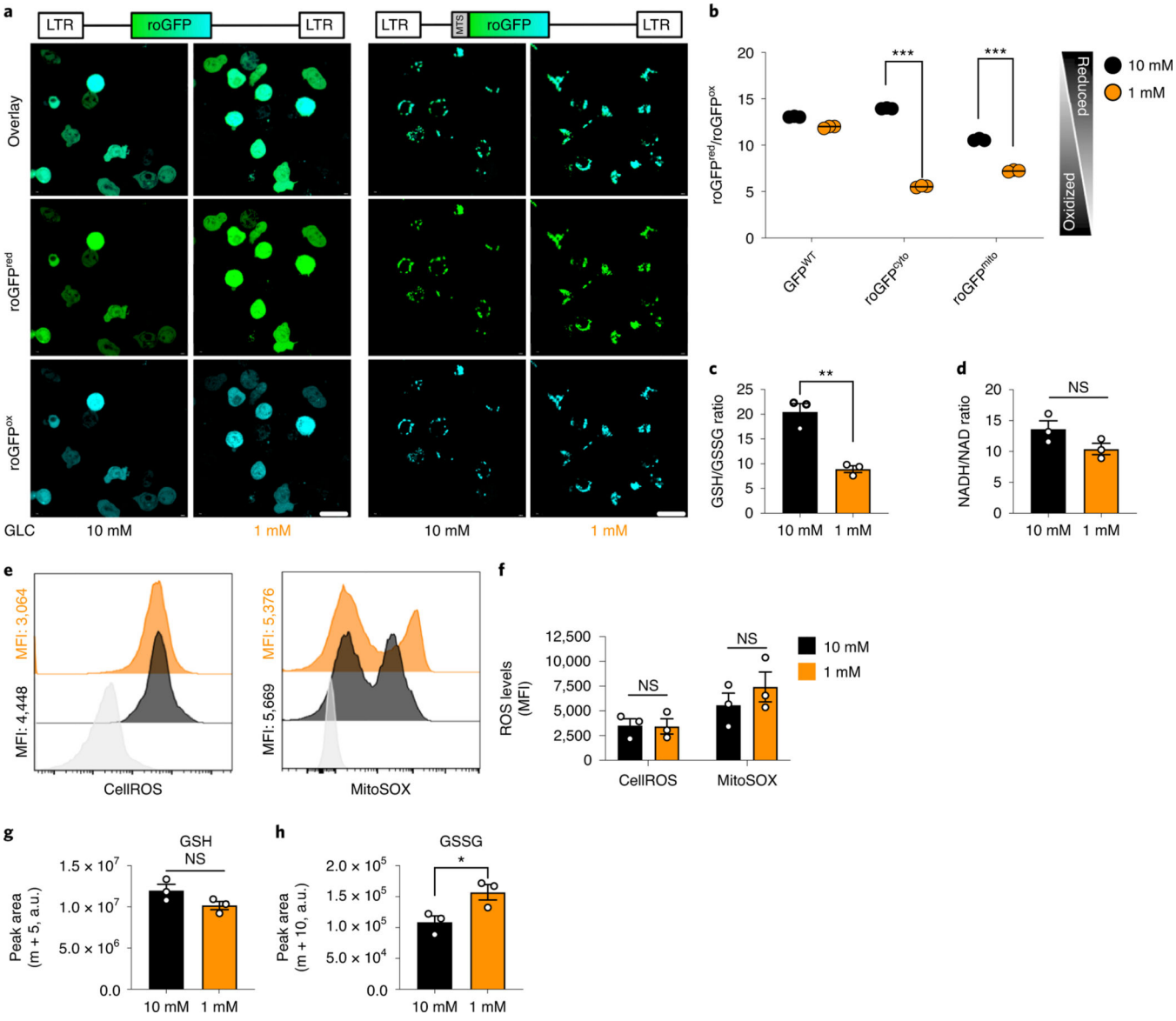

Fig. 4. TGR T_E have reversible redox balance without accumulating cellular ROS.

(**a-b**) WT $CD8^+$ T cells were activated with anti-CD3 (5 mg/mL), anti-CD28 (0.5 mg/mL), and IL-2 (100 U/mL) for 36h, transduced with retrovirally encoded roGFP or mitochondrially-targeted roGFP (MOI=1), expanded for 36 hours and exposed to 10mM (black) or 1mM (orange) glucose for 20h in cultures set to 1 million per ml. (**a**) Micrographs show cytosolic roGFP and mitochondrial roGFP localization assessed with confocal microscopy (scale bar 10μm). (**b**). Flowcytometric quantification of signal ratios, taking the derived parameter per cell (488nm-excited (reduced roGFP) / 405nm-excited (oxidized roGFP). WT-GFP was used as a control. (**c-d**) Polar metabolites were extracted from cells as generated in Fig. 2f, analyzed using a QTOF mass spectrometer. Redox-couple ratios were computed in extracts from cells grown in 10mM (black) or 1mM (orange) glucose. (**c**) ratio of reduced glutathione (GSH) / oxidized glutathione (GSSG). (**d**) ratio of reduced nicotinamide adenine dinucleotide (NADH) / oxidized dinucleotide (NAD^+). (**a-d**)

Data shown for n=3 biological replicates, representative of 3 independent experiments. (**e**) Reactive oxygen species (ROS) were assessed by incubation of control T_E (black) and TGR T_E (orange) in cellular ROS dye (CellROS, left panel) or mitochondrial ROS dye (MitoSOX, right panel). Staining levels were measured by flow cytometry and compared to unstained cells (grey). Histograms represent 3 biological replicates. (**f**) Quantification of the histograms shown in (e) showing n=3 biological replicates. (**g-h**) WT $CD8^+$ T cells isolated from spleens of C7Bl/6 mice were activated with anti-CD3 (5 mg/mL), anti-CD28 (0.5 mg/mL), IL-2 (100 U/mL), expanded for a total of 72 hours, and exposed to 10mM (black) or 1mM (orange) glucose and U-^{13}C-glutamine in cultures set to 1 million per ml.. Cells were washed in cold PBS and polar metabolites were extracted. Samples were measured by LC-MS and peak areas for (**g**) the m+5 isotopologue of GSH and (**h**) the m+10 isotopologue of GSSG were extracted. Data of n=3 biological replicates. (**b-h**) Significance was calculated using 2-tailed Student's *t* tests, ns; non-signifcant, * $p<0.05$; ** $p<0.01$; *** $p<0.01$. All error bars show SEM.

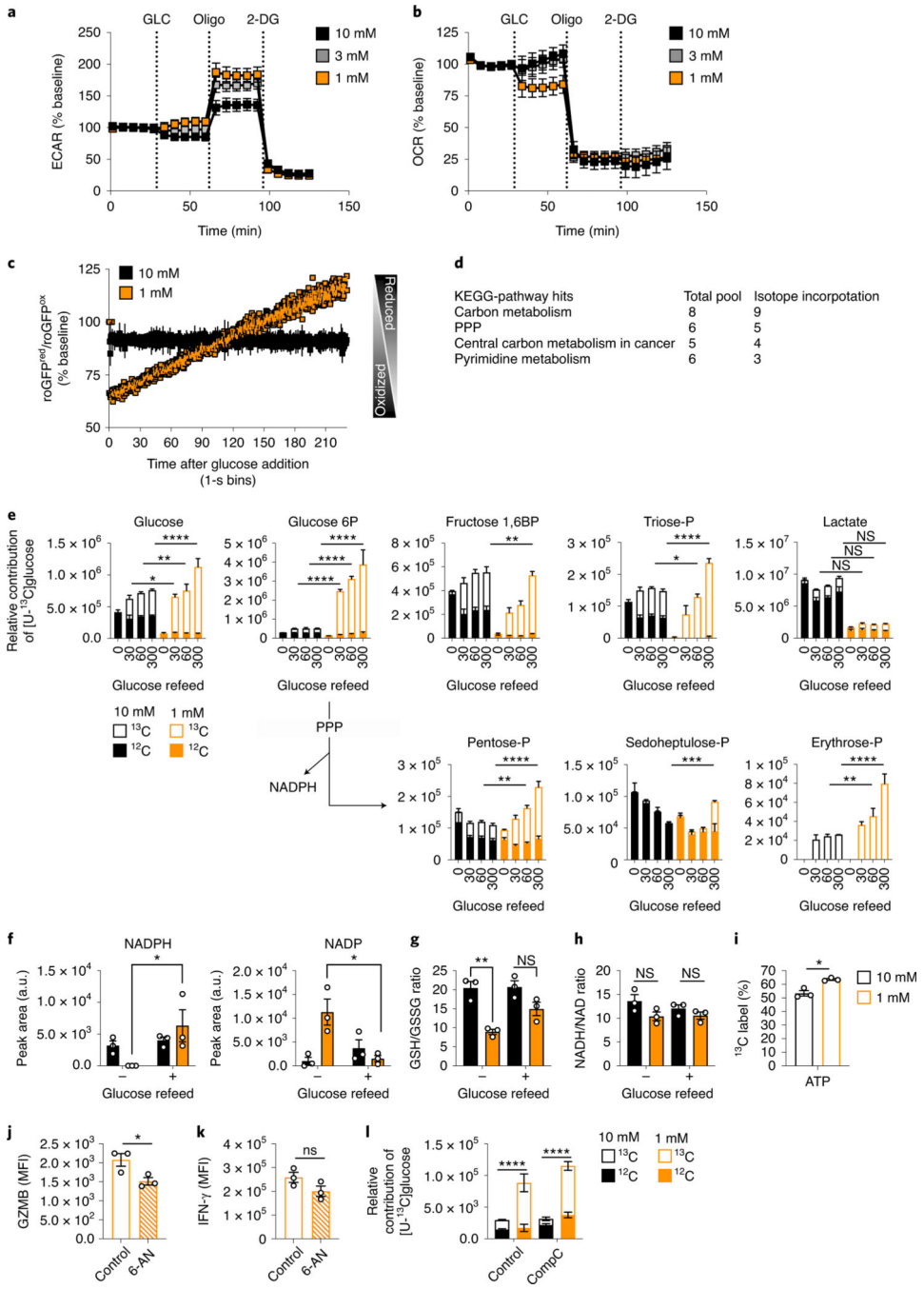

Fig. 5. TGR CD8$^+$ T_E have enhanced anabolic metabolism upon glucose re-exposure.

T_E were generated as in (Fig. 2f). (**a**) Basal ECAR and (**b**) basal OCR (percentage of baseline) with 10mM glucose (GLC), Oligomycin (Oligo), and 2-deoxyglucose (2-DG) treatment. Data shows average of n=3 biological replicates. (**c**) roGFP$^+$ control (black) or TGR (orange) T_E generated as in (Fig. 3a–b) were pulsed with 10mM glucose. roGFP ratios were measured continuously for 5-mins. Data depicts average normalized ratio in 1-second bins from n=3 biological replicates. (**d-e**) Table depicts overlapping Kegg-Pathway hits with increased total pool size and ^{13}C incorporation in TGR-treated T_E following

5-minute glucose re-exposure. (**e**) control (black) or TGR (orange) T_E were pulsed with 10mM U-^{13}C-glucose for 30, 60, and 300 seconds. 20h cultures were started at 1×10^6 (control) and 1.5×10^6 (TGR) cells per/ml to generate similar end concentrations for glucose pulse experiments. Data are averages from n=3 biological replicates. Statistical significance was calculated using 2way-ANOVA, shown for U-^{13}C allocation of time-matched pairs. * p<0.05, ** p<0.01; *** p<0.001; **** p<0.0001. (**f**) Reduced nicotinamide-adenine-dinucleotide-phosphate (NADP) and oxidized nicotinamide-adenine-dinucleotide-phosphate (NADPH). (**g**) Ratio of reduced glutathione (GSH)/oxidized glutathione (GSSG). (**h**) Ratio of reduced NADH/oxidized NAD. (**f-h**) Significance was calculated using 2-tailed Student's *t* tests on n=3 biological replicates. ** p<0.01; * p<0.05; ns=not significant. (**i**) Percent ^{13}C labeled ATP derived from 6h ^{13}C-glucose re-exposure. Significance was calculated using 2-tailed Student's *t* tests on n=3 biological replicates. * p<0.05. (**j**) TGR T_E were pretreated with solvent or 6-aminonicotinamide (6-AN, 250 μM) for 30 minutes, followed by re-stimulation using PMA/ionomycin + 6-AN, 10mM glucose and brefeldin-A, and assessed for (**j**) intracellular GZMB and (**k**) IFN-γ. Data shows n=3 biological replicates, significance was calculated by 2-tailed Student's *t*-test. * p<0.05. (**l**) T_E pretreated with control or AMPK-inhibitor (CompC, 10 μM) for 30 minutes were pulsed with U-^{13}C-glucose for 5 minutes followed by polar metabolite extraction. Incorporation of ^{13}C label in Pentose-phosphate was measured by LC-MS. Data show on n=3 biological replicates, significance was calculated by 2way-ANOVA. Significance is shown for relative ^{13}C incorporation (open bars). **** p<0.001. All data panels are representative of 3 independent experiments, all error bars show SEM.

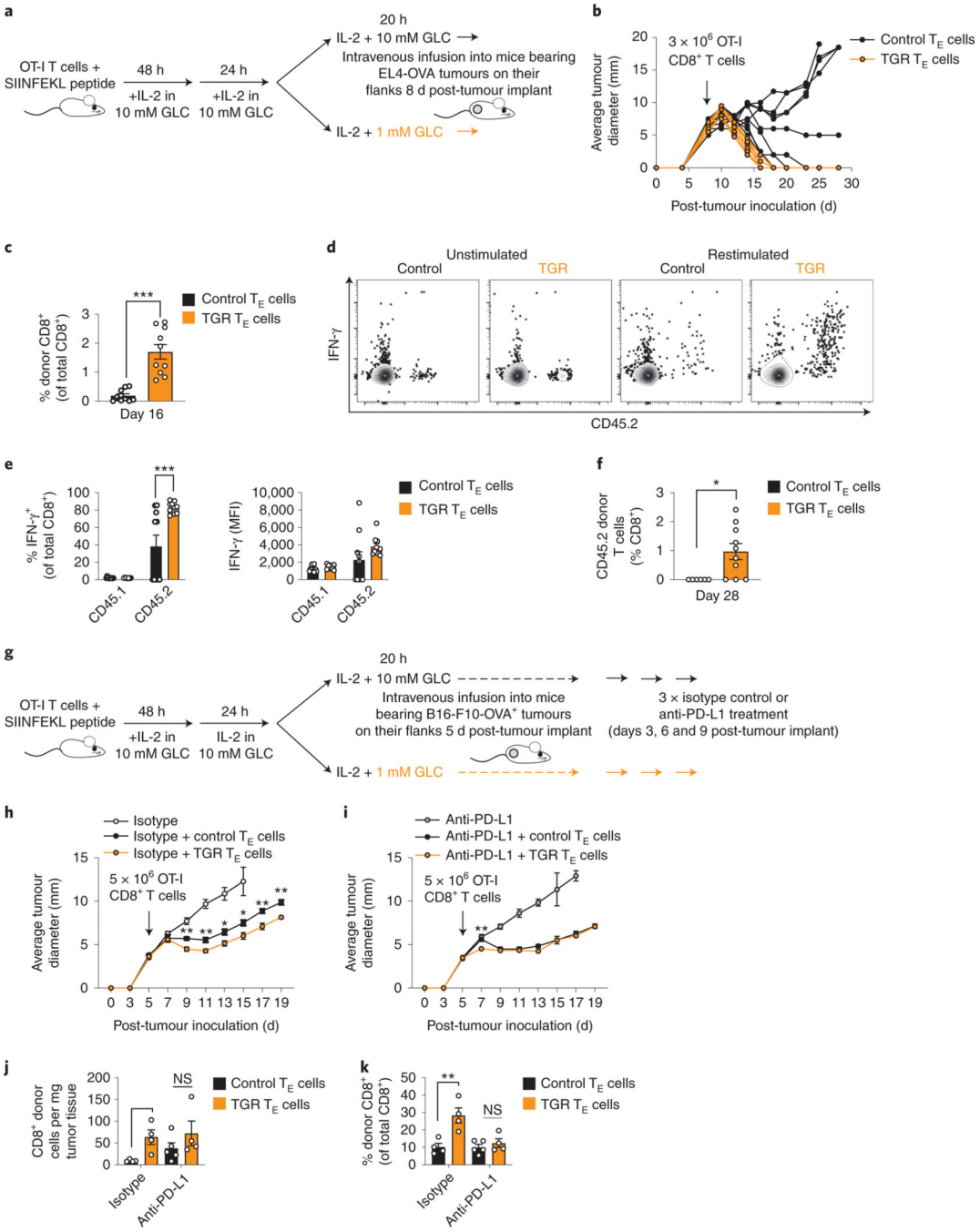

Fig. 6. TGR enhances tumor-specific CD8$^+$ T_E function *in vivo*.

(**a**) Ova-specific CD8$^+$ T cells (OT-I) from CD45.2 female mice were activated by SIINFEKL peptide and IL-2 (100 U/mL), expanded for 72h, then exposed to 20h to 10mM (Control, black) or 1mM (TGR, orange) glucose. CD45.1 female recipient mice were injected with 1×10^6 E.G7-OVA lymphoma cells, tumors were established for 8 days, and 3 ×10^6 OT-I$^+$ T_E were injected per tumor bearing mouse. (**b**) Average tumor diameter of control (black n=9) or TGR (orange n=10) T_E recipient animals. (**c-e**) Blood was collected 16 days post tumor injection and the percent and function of donor (CD45.2) CD8$^+$ T

cells was assessed by (**c**) congenic markers and (**d-e**) IFN-γ expression after re-stimulation with PMA/ionomycin + brefeldin-A. (**f**) Blood was collected day 28 post tumor injection to assess percent of donor (CD45.2) $CD8^+$ T cells. (**c-f**) Statistical significance was calculated on n=9 and n=10 animals by 2-tailed Student's *t*-test. * $p<0.05$; *** $p<0.001$. (**g**) T_E cells were generated as described in (**a**). CD45.1 female recipient mice were injected subcutaneously with 1×10^6 B16-OVA melanoma cells and tumors established for 5 days. 5×10^6 control (black) or TGR (orange) OT-I^+ T_E were injected intravenously per tumor bearing mouse. Mice receiving no T_E were used as control. 3, 6 and 9 days after tumor inoculation, mice received 200 μg anti-PD-1 antibody or lgG2a isotype control in 100 μl PBS intraperitoneally. (**h-i**) Lines depict average tumor diameter of grouped mice. Statistical significance was calculated by multiple 2-tailed Student's *t* tests comparing control T_E and TGR T_E over the timecourse on n=5 animals. * $p<0.05$; ** $p<0.01$. (**j-k**) 21 days after tumor inoculation mice were humanely euthanized and the tumor mass was excised. Single cell suspensions were analyzed by flow cytometry. The number of donor (CD45.2) $CD8^+$ T cells per mg tissue (**j**) and the percent of donor (CD45.2) $CD8^+$ T cells (**k**) was quantified. Statistical significance was calculated by 2-tailed Student's *t* test. * $p<0.05$; ** $p<0.01$. Tumor size measurements were performed by blinded researchers. All error bars show SEM.